UNIVERSITAT POLITÈCNICA DE CATALUNYA
BARCELONATECH
Escola d'Enginyeria de Telecomunicació
i Aeroespacial de Castelldefels

POLITECNICO
DI TORINO

TREBALL DE FI DE GRAU

TFG TITLE: Small Satellite Attitude and Orbital Control for Precise Pointing Missions

DEGREE: Bachelor's Degree in Aerospace Systems Engineering

AUTHOR: Julián Sintes Garcia

ADVISORS: Elisa Capello
Jordi Gutiérrez Cabello

DATE: August 13, 2020

Títol: Control d'Actitud i Orbital d'un Satèl·lit per a Missions d'Apuntament Precís
Autor: Julián Sintes Garcia

Directors: Elisa Capello
Jordi Gutiérrez Cabello

Data: 13 d'agost de 2020

Resum

Des de la Guerra Freda entre els Estats Units i la Unió Soviètica, la tecnologia del sector espacial ha millorat molt. Actualment, els satèl·lits són utilitzats en diferents aplicacions, com pot ser comunicacions, navegació, satèl·lits d'observació, etc. A més a més, l'avanç tecnològic que hem viscut durant aquestes darreres dècades ens ha permès una notable reducció del tamany i del pes dels satèl·lits, i per tant una reducció del seu alt cost. Això ha provocat un augment en el llançament d'aquets objectes, que tenen un temps de vida útil determinat i que majoritàriament, una vegada aquesta vida s'acaba queden orbitant en forma d'escombraries espacials.

El principal objectiu d'aquesta recerca es el disseny d'un sistema de control de la dinàmica orbital i d'actitud d'un satèl·lit per a missions d'apuntat precís, tant de recollida de dades d'alguns objectes celestes com de la captura d'escombraries espacials orbitant al voltant de la Terra.

Per començar, al Capítol 1 es fa una breu explicació sobre els principals conceptes teòrics necessaris per realitzar aquest treball: els sistemes de coordenades de referència considerats, les equacions que descriuen la dinàmica orbital (equacions de Hill) i d'actitud (equacions d'Euler) del satèl·lit, sistemes d'actuació, etc.

Per altra banda, al Capítol 2 es fa una descripció del concepte de rendezvous a l'espai i de totes les seves fases. A més a més també descriu els dos casos pràctics amb els que es comprovarà l'eficiència del sistema i el satèl·lit 12U CubeSat 1HOPSat de l'empresa Hera Systems, que s'utilitzarà com a model de referència per realitzar les simulacions dels dos escenaris.

Com és veurà al Capítol 3, un dels elements principals del sistema de control orbital és la funció de guiatge. Dos algoritmes de guia diferents s'han seleccionat: Proportional Navigation Guidance i Control Terminal Velocity Guidance. A més a més, també es fa una breu descripció del controlador que s'utilitzarà per manejar l'actitud del satèl·lit, un controlador Proporcional-Derivatiu.

Finalment, al Capítol 4 es mostren les simulacions obtingudes d'ambdues missions i es comenten els principals resultats obtinguts.

Paraules clau: Satèl·lit, Rendezvous, Control, Guiatge, GNC

Title : Small Satellite Attitude and Orbital Control for Precise Pointing Mission
Author: Julián Sintes Garcia

Advisors: Elisa Capello
Jordi Gutiérrez Cabello

Date: August 13, 2020

Overview

Since the Cold War between the United States and the Soviet Union, space sector technology has greatly improved. Today, satellites are used in different applications such as communications, navigation, observation satellites, and more. In addition, the technological advancement we have experienced in recent decades has allowed us to significantly reduce the size and weight of satellites, and therefore a reduction in their high cost. This has led to an increase in the launch of these objects, which have a certain useful life time and once they end up, they are mostly orbited in the form of space debris.

The main objective of this research is the design of the control system for both orbit and attitude dynamics of a small satellite for precise pointing missions, both for collecting data from celestial objects and the capture of space debris orbiting the Earth.

To begin with, Chapter 1 gives a brief explanation of the main theoretical concepts needed to carry out this thesis: the considered reference coordinate frames, the equations that describe orbital (Hill's equations) and attitude (Euler's equations) dynamics of the satellite, actuation systems, etc.

On the other hand, Chapter 2 describes the concept of space rendezvous and all the phases. It also describes the two practical cases that will test the efficiency of the system and the satellite 12U CubeSat 1HOPSat from Hera Systems, which will be used as a reference model to perform the simulations of the two scenarios.

As it will be seen in Chapter 3, one of the main elements of orbital control system is the guidance function. Two guidance algorithms are selected: Proportional Navigation Guidance and Control Terminal Velocity Guidance. In addition, the attitude controller is briefly described, which is a Proportional Derivative controller.

Finally, Chapter 4 shows the simulations obtained from both missions and discusses the main results.

Keywords: Satellite, Rendezvous, Control, Guidance, GNC

Dedicat a sa família i es amics

CONTENTS

LIST OF FIGURES

LIST OF TABLES

INTRODUCTION

The human being always has had an intrinsic interest in exploring and knowing outer space. During the first centuries b.C., in Ancient Greece there were already scientists that wanted to know the unknown, and started carrying out the first astronomical-scientific works: Eudoxus of Cnidus proposed for the first time the geocentrical model and later was supported by Aristotle, or Aristarchus of Samos, that calculated for the first time the distance from Earth to the Moon and the Sun and proposed an heliocentric model [1, 2].

However, it wasn't until the early modern period with the scientific revolution when started the most significant discoveries in astronomy. Nicolaus Copernicus worked on his heliocentric theory for a long period of his life but it was not accepted by many other scholars of the epoch since this constituted a whole scientific revolution. A few years later, Johaness Kepler could announce the laws of planetary movement with the help of the astronomical measurements carried out by Tycho Brahe some years before. At the same time, one of the most important scientists of the time, Galileo Galilei, was able to build his own observation instruments, nevertheless there were no technology that could make possible to go out and explore everything around us [3].

The early era of space exploration was driven by a "Space Race" between two Cold War rivals, the Soviet Union and the United States, that lasted from 1947 to 1991 with the dissolution of the Soviet Union. During this period, both states were competing to achieve firsts in spaceflights capability, and started working in rocket development independently. Then, it was the Soviets who took head carrying out both the first outer space flight and the first human space flight, however, it was the Americans who made the first astronomical body space explorations with the Apollo missions [4].

From the first successful artificial satellite, Sputnik 1 [5], launched by the Soviet Union in 1957, about 8900 satellites has been launched from more than 40 countries used for so many different purposes: Earth observation, communications, navigation, weather satellites, etc. In 2018 it was estimated that only about 1900 were still operational and the most of the part of the others have become space debris [6].

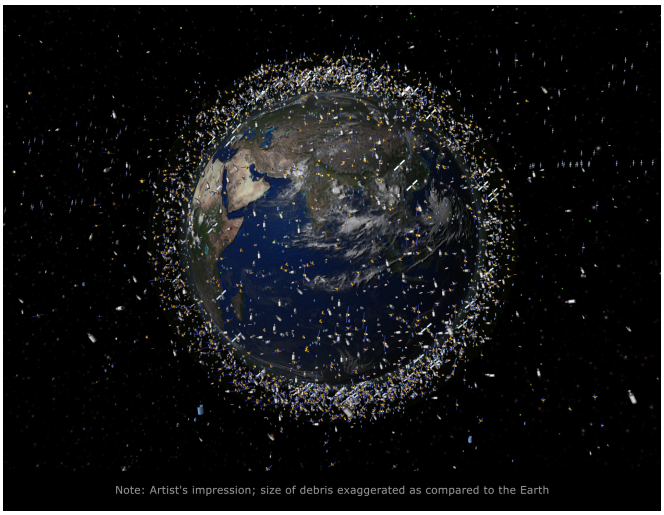

Figure 1: Artist's impression with exaggerated size of debris objects in low-Earth orbit. Source: ESA, 2008

Thus, accumulation of space junk during last decades has supposed a relevant problem for new space missions because of the increase of the risk in orbital collisions. Low-Earth orbit (LEO) has developed into an orbital graveyard, so that space agencies have started to develop space missions such as the ClearSpace-1 mission [7] by ESA or the End-of-Life Service by AstroScale (ELSA) [8] to clean up space using small cube-shaped satellites. However, since these spacecraft are subject to strict requirements in terms of angular position and actuation limits, advanced control algorithms are usually designed to combine robustness properties and limited control effort, including external disturbances and parametric uncertainties.

The main objective of this research is the design a control system for both orbit and attitude dynamics of a small satellite intended for precise pointing missions, following the classical blocks diagram of the Guidance, Control and Navigation (GNC) subsystem of the onboard computer defined in [12].

To begin with, it will be necessary to study some theoretical concepts, briefly explained in the first chapter, needed to carry on the thesis. Since a rendezvous manoeuvre between a Chaser and Target is considered, Hill's equations extensively described in [12] are used to analyze the relative motion between both spacecraft. Also, for the attitude kinematics, instead of using Euler angles [13] that is very computationally intense, a quaternion representation, based in Euler's rotational theorem, explained in [16, 17] is considered and the Euler's equations defined in [14, 18] are used to evaluate the attitude dynamics of the chaser. Finally, a short definition from [20, 22] of the actuation systems that are used.

Then, in order to evaluate the orbit control system, several guidance algorithms will be implemented and tested to prove their effectiveness. From a classical Proportional Navigation law defined in [30, 31, 32], originally used in homing missiles during World War II and, then, extrapolated to space operations such as asteroid rendezvous, to a more modern optimal algorithm called Control Terminal Velocity Guidance from [33, 34]. On the other side, the attitude control system will be evaluated by implementing a simple Proportional-Derivative controller, a feedback control mechanism widely used in many industrial control systems.

So as to evaluate the proposed control system, two different practical cases from [22] are considered as reference and extended simulations are carried out to show the performance of the system.

CHAPTER 1. MATHEMATICAL MODEL AND PROBLEM SETUP

In order to model the advanced guidance and control algorithms that control the orbital and attitude dynamics of a spacecraft, some theoretical concepts from mathematics and classical mechanics must be studied to understand the behaviour of spacecraft.

Among these concepts, we can find the Hill's equations that describe the relative motion between two spacecraft, the Euler's equations and quaternions that describe the attitude rigid body dynamics and kinematics and also the reference frames that these equations are expressed in, among others.

1.1. Reference coordinate frames

The equations of motion, used for studying dynamics and kinematics of the spacecraft, are defined in different reference frame: (1) the kinematics is defined by an inertial frame, (2) the orbit dynamics is defined in a local orbital frame (Local Vertical Local Horizontal, LVLH) and (3) finally, the attitude dynamics is expressed in a body reference frame.

1.1.1. Earth Centered Inertial frame

The Earth Centered Inertial (ECI) frame $(X_{ECI}, Y_{ECI}, Z_{ECI})$ is an inertial frame rotating with the Earth. Its origin is set at the CoM (Center of Mass) of the planet and is described by:

- X-axis points towards the vernal equinox.
- Z-axis is Earth's rotation axis, perpendicular to equatorial plane (pointing in the direction of the north pole).
- Y-axis is in the equatorial plane, forming a right-handed coordinate system.

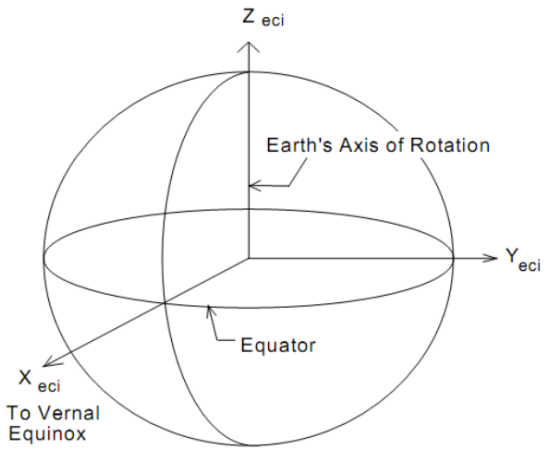

Figure 1.1: Earth Centered Inertial (ECI) Coordinate System [9]

1.1.2. Spacecraft local orbital frame

When a space rendezvous manoeuvre, in which one spacecraft (Chaser) is about to meet another one following a certain and well known orbit (Target) yet, is about to be performed the spacecraft local orbital frame or LVLH frame $(V_{bar}, H_{bar}, R_{bar})$ of the target is considered. It is the reference coordinate system of the Hill's equations. Since it is rotating at an angular velocity with respect to the ECI frame, it is considered a pseudo-inertial reference frame for relative motion and is described by:

- The origin is set at the CoM of the target spacecraft.
- Z-axis (Local Vertical), or R_{bar}, points towards the center of the Earth.
- X-axis (Local Horizontal), or V_{bar}, is in the direction of orbital motion of the satellite and it's tangent to the orbit.
- Y-axis, or H_{bar}, it's perpendicular to the orbital plane, forming a right-handed coordinate system.

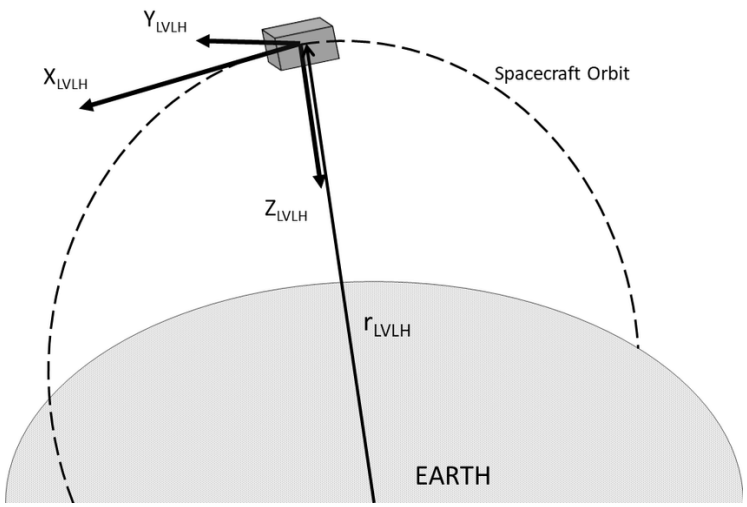

Figure 1.2: Spacecraft local orbital frame [10]

1.1.3. Spacecraft attitude frame

In the Euler's equations for the spacecraft body dynamics (see section 1.3.4.), the used reference frame is the spacecraft attitude frame, also called body reference frame (X_B, Y_B, Z_B). It is defined by:

- The origin is set at the CoM of the chaser spacecraft.
- In a cube-shaped spacecraft, the axes should be popping out perpendicularly from the different faces of the satellite.
- It is rotated from the local orbital frame of the chaser by the attitude angles (see section 1.3.1.).

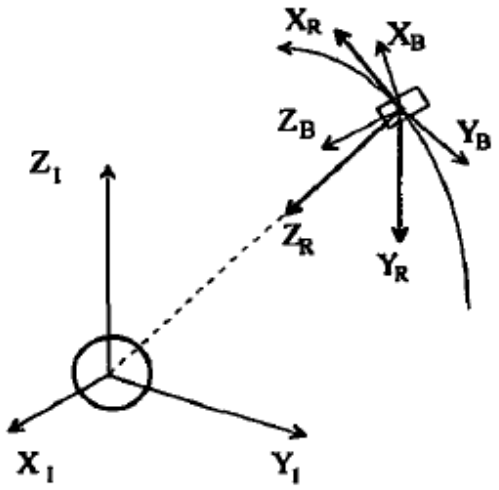

Figure 1.3: Spacecraft attitude frame [11]

1.2. Orbital dynamics

1.2.1. Hill's equations

For the analysis of rendezvous trajectories, the equations of motion around a central body derived from Kepler's and Newtons laws are only used until the chaser spacecraft is located close to the target. Beyond this point, it is more convenient to keep one of the spacecraft as a fixed point.

Then, as briefly said before, the reference coordinate system is the spacecraft local orbital frame with its origin located at the center of mass of the target vehicle. The following equations, called **Hill's equations** [12], describe the relative motion between the target and the chaser:

$$\ddot{x} = \frac{1}{M_c}F_x + 2\omega\dot{z} \tag{1.1}$$

$$\ddot{y} = \frac{1}{M_c}F_y - \omega^2 y \tag{1.2}$$

$$\ddot{z} = \frac{1}{M_c}F_z - 2\omega\dot{x} + 3\omega^2 z \tag{1.3}$$

In these equations, ω is the orbital angular velocity of the target, M_c is the mass of the chaser, $\mathbf{x} = [x, y, z]^T$ and $\dot{\mathbf{x}} = [\dot{x}, \dot{y}, \dot{z}]^T$ are the current position and relative velocity of the chaser, respectively, and $\mathbf{F} = [F_x, F_y, F_z]^T$ is the force that must be applied by the actuation system. Anyways, from now on we will no longer speak of force but of the acceleration that must be applied, which is denoted as $\gamma = \mathbf{F}/M_c = [\gamma_x, \gamma_y, \gamma_z]^T$. However, the equations are subject to the following assumptions:

- Only circular orbits are analyzed.
- The distance between the chaser and the target is lower than the orbital radius.

1.3. Attitude kinematics and dynamics

1.3.1. Euler angles

The orientation of a mobile reference system, F_b, with respect to another fixed frame, F_a, can be described with three finite rotations about three axes, a set of three angular coordinates $[\Phi, \Theta, \Psi]$ called **Euler angles** [13], referred also as the **attitude angles**, and each of these rotations has an associated rotation matrix R_i (Eqs. 1.4-1.6). In aeronautics, these rotations are done taking into account the following conventions:

- It is used the convention ZYX, also called 321 or Tait-Bryan.
- Positive rotations are done in the anticlockwise direction.

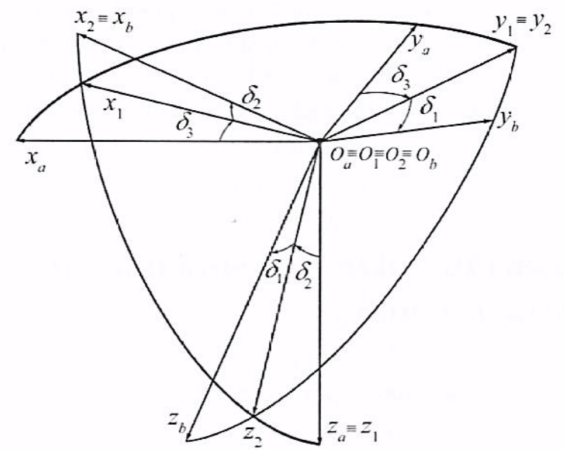

Figure 1.4: Euler angles with ZYX convention [13]

Then, these are the rotation matrices that describe each of the turns about each of the three axes:

$$R_1 = \begin{bmatrix} 1 & 0 & 0 \\ 0 & \cos\phi & \sin\phi \\ 0 & -\sin\phi & \cos\phi \end{bmatrix} = [\Phi] \tag{1.4}$$

$$R_2 = \begin{bmatrix} \cos\theta & 0 & -\sin\theta \\ 0 & 1 & 0 \\ \sin\theta & 0 & \cos\theta \end{bmatrix} = [\Theta] \tag{1.5}$$

$$R_3 = \begin{bmatrix} \cos\psi & \sin\psi & 0 \\ -\sin\psi & \cos\psi & 0 \\ 0 & 0 & 1 \end{bmatrix} = [\Psi] \tag{1.6}$$

That is, in order to express a vector in the frame F_b knowing its coordinates in the frame F_a, we must use the transformation matrices defined above as follows:

$$\vec{v_b} = [\Phi][\Theta][\Psi]\vec{v_a} = L_{ba}\vec{v_a} \tag{1.7}$$

where the product of the three matrices gives the transformation matrix from one frame to another, also called **attitude matrix**:

$$L_{ba} = \begin{bmatrix} c\theta c\psi & c\theta s\psi & -s\theta \\ s\phi s\theta c\psi - c\phi s\psi & s\phi s\theta s\psi + c\phi c\psi & s\phi c\theta \\ c\phi s\theta c\psi + s\phi s\psi & c\phi s\theta s\psi - s\phi c\psi & c\phi c\theta \end{bmatrix} \tag{1.8}$$

1.3.2. Euler parameters

As the **Euler Theorem for Rotations** states, *the general displacement of a rigid body with one fixed point is a rotation about some axis* [14].

This means that any rotation about the three axes can be described by a single rotation angle or **Euler angle**, α, about the principal axis or **Euler axis**, $\hat{\mathbf{E}}$, defined as the axis that passes through the origin and a point that remains fixed (see Figure 1.5).

Thus, once this theorem is applied, the rotation matrix described in the previous section, L_{ba}, results as:

$$L_{ba} = \cos\alpha \mathbf{1} + (1 - \cos\alpha)\mathbf{E}\mathbf{E}^T + \sin\alpha \mathbf{E}^\times \tag{1.9}$$

However, it follows from the Euler theorem that the relative orientation of any pair of coordinate systems can be specified by a set of three independent numbers, $\mathbf{q}_v = [q_1, q_2, q_3]$, but sometimes also a fourth redundant number, q_0, is added to simplify the operations with quaternion algebra. This set of four numbers is called **quaternion**, $\mathbf{q} = [q_1, q_2, q_3, q_0]^T$.

$$\begin{aligned} \mathbf{q}_v &= \hat{\mathbf{E}} \sin\frac{\alpha}{2} \\ q_0 &= \cos\frac{\alpha}{2} \end{aligned} \tag{1.10}$$

The main advantage of using quaternions instead of the axis-angle parameters is that the expression for the rotation matrix and kinematics is purely algebraic. Then, the rotation matrix expressed with quaternions is:

$$L_{ba} = (2q_0^2 - 1)\mathbf{1} + 2\mathbf{q}_v\mathbf{q}_v^T - q_0\mathbf{q}_v^\times \tag{1.11}$$

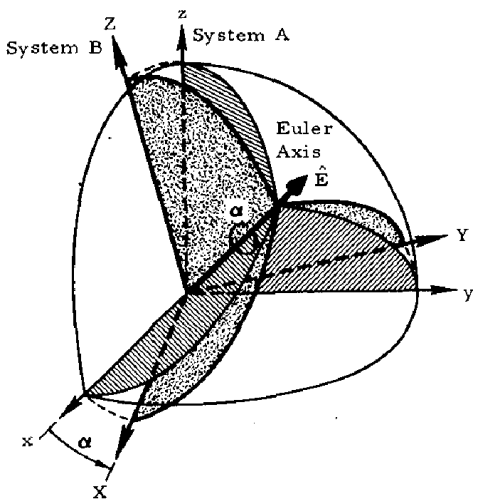

Figure 1.5: Euler theorem for rotations [15]

1.3.3. Kinematic equations

Navigation and control for spacecraft flying requires the relative attitude information. The attitude of a rigid-body with respect to the inertial frame is determined by a rotation transformation matrix from the inertial frame to body frame. Similarly, rotation matrix of the body-frame with respect to a non-inertial frame can be defined as the relative attitude matrix and, in developing the kinematics and dynamics of the relative attitude the kinematic equations are addressed [16].

If Euler angles are used to describe the angular rates of the spacecraft attitude the equations are:

$$\dot{\phi} = \omega_x + \omega_y \sin\phi \tan\theta + \omega_z \cos\phi \tan\theta \tag{1.12}$$

$$\dot{\theta} = \omega_y \cos\phi - \omega_z \sin\phi \tag{1.13}$$

$$\dot{\psi} = \frac{\omega_y \sin\phi}{\cos\theta} + \frac{\omega_z \cos\phi}{\cos\theta} \tag{1.14}$$

As can be observed, some of the angular rates become quite large when θ approaches $\frac{\pi}{2}$ or $\frac{3\pi}{2}$, and in fact go to infinite when $\theta = \frac{\pi}{2}$ or $\frac{3\pi}{2}$. This problem is called a kinematic singularity and it is a major disadvantage of using Euler angles. Besides, it is computationally expensive to compute the sines and cosines needed to integrate Eqs. 1.12-1.14.

On the other side, in terms of the Euler axis/angle attitude parameters (see section 1.3.2.), the kinematic equations of motion look as follows:

$$\dot{\mathbf{E}} = \frac{1}{2}\left[\mathbf{E}^{\times} - \cot\frac{\alpha}{2}\mathbf{E}^{\times}\mathbf{E}^{\times}\right]\omega \tag{1.15}$$

But once again, there is an evident singularity in these equations at $\alpha = 0$ or 2π, which means that the two frames are identical.

To avoid all these singularities the Euler parameters or quaternions are also frequently used to describe the kinematic of spacecraft. Thus, the differential equations that describes the propagation of quaternions with time are:

$$\dot{q} = \frac{1}{2}\mathbf{Q}\omega \tag{1.16}$$

where ω is the vector of the angular velocity of the spacecraft $[\omega_x, \omega_y, \omega_z]$ and $\mathbf{Q}$ is the quaternion matrix defined as:

$$\mathbf{Q} = \begin{bmatrix} -q_1 & -q_2 & -q_3 \\ q_0 & -q_3 & q_2 \\ q_3 & q_0 & -q_1 \\ -q_2 & q_1 & q_0 \end{bmatrix} \tag{1.17}$$

Even so, there are some books that also uses other formulations for the differential equation of quaternions. For example the one proposed in [17]:

$$\dot{q} = \frac{1}{2}F_q(\omega)\mathbf{q} = \frac{1}{2}\begin{bmatrix} 0 & -\omega_x & -\omega_y & -\omega_z \\ \omega_x & 0 & \omega_z & -\omega_y \\ \omega_y & -\omega_z & 0 & \omega_x \\ \omega_z & \omega_y & -\omega_x & 0 \end{bmatrix} \cdot \begin{bmatrix} q_0 \\ q_1 \\ q_2 \\ q_3 \end{bmatrix} \tag{1.18}$$

Most of the time, it is requested to go from an initial to a final attitude state. For that purpose, it is suitable to compute the deviation between the actual and the desired attitude, that is, the **quaternion error**. As an attitude quaternion is derived directly from the attitude matrix, the quaternion error cannot be computed as a simple difference, the allowed operations are the matrix multiplications:

$$q_{err} = q_{des}^{-1} \otimes q_{act} \tag{1.19}$$

where the quaternion inverse and the quaternion multiplication are computed, respectively:

$$q^{-1} = \frac{[q_0^2 \ -q_1^2 \ -q_2^2 \ -q_3^2]^T}{q_0^2+q_1^2+q_2^2+q_3^2} \tag{1.20}$$

$$p = q \otimes r = \begin{bmatrix} q_0 & -q_1 & -q_2 & -q_3 \\ q_1 & q_0 & -q_3 & q_2 \\ q_2 & q_3 & q_0 & -q_1 \\ q_3 & -q_2 & q_1 & q_0 \end{bmatrix} \cdot \begin{bmatrix} r_0 \\ r_1 \\ r_2 \\ r_3 \end{bmatrix} \tag{1.21}$$

Since understanding the physical meaning of quaternions is not that easy, it is useful to use Euler angles to understand the attitude variation:

$$\phi = \arctan\left[\frac{2(q_0q_1+q_2q_3)}{1-2(q_1^2+q_2^2)}\right] \tag{1.22}$$

$$\theta = \arcsin[-2(q_1q_3-q_0q_2)] \tag{1.23}$$

$$\psi = \arctan\left[\frac{2(q_1q_2+q_0q_3)}{1-2(q_2^2+q_3^2)}\right] \tag{1.24}$$

1.3.4. Euler's equations

For the evaluation of the angular rates of spacecraft, the classical **Euler's equations** [14, 18] that describes the rotation dynamics of a rigid body are considered. In these equations, as has been said in the section 1.1.3., the reference frame is the body frame.

With this purpose, in the moment equations have to be considered the moments produced by the thrusters, the reaction wheels and all the external disturbances that affect to the spacecraft. Thus, the following formula describes the attitude angular rates in the most general way, that means that it is valid for any set of body-fixed axes:

$$\dot{\omega}_B = I^{-1}(M_B - \omega_B \times (I\omega_B + I_{RW}\omega_{RW})) \tag{1.25}$$

where I and I_{RW} are the inertia tensors of the spacecraft and the reaction wheels, respectively; M_B is the total moment acting on the chaser, that is all the external disturbances and the moment because of the thursters and the reaction wheels; and ω_B and ω_{RW} are the angular velocities of the satellite and the reaction wheels, respectively.

Considering the principal axis of the spacecraft and equating the angular velocity rate about each of the axes, we get the the following equations, known as the **Euler's equations**, expressed in terms of moments of inertia about the principal axes:

$$\dot{\omega}_x = \frac{1}{I_{xx}}(M_x + (I_{yy}-I_{zz})\omega_y\omega_z) \tag{1.26}$$

$$\dot{\omega}_y = \frac{1}{I_{yy}}(M_y + (I_{zz} - I_{xx})\omega_z\omega_x) \tag{1.27}$$

$$\dot{\omega}_z = \frac{1}{I_{zz}}(M_z + (I_{xx} - I_{yy})\omega_x\omega_y) \tag{1.28}$$

1.4. Actuation systems

The Attitude and Orbit Control System (AOCS) of a spacecraft can be defined as the set of actuators that allows to control the translational and rotational dynamics of the vehicle. The actuators may be divided in two groups: position actuation systems and attitude actuation systems [20].

1.4.1. Propulsion system

The propulsion system of a spacecraft is composed of a grouping of thrusters that allows to control the movement of the satellite in all three axes, independently of an ambient magnetic and gravitational field. Depending on the functions that have to be performed and then constraints of the mission, there are different kinds of thrusters: cold gas thrusters, ion thrusters, Hall effect thrusters, etc.

In the most of the cases, proportional control is not feasible, that is thrusters are not able to produce any value of force and are ON/OFF devices. This type of control signal is usually referred to as **Pulse-Width Modulation** (PWPF) [21].

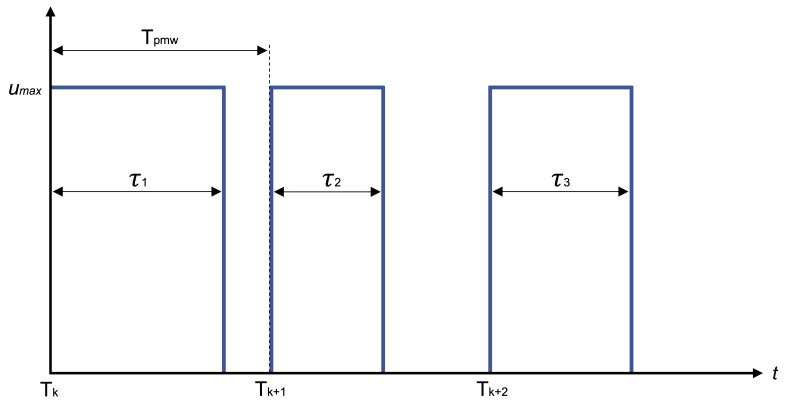

Figure 1.6: Pulse-Width Modulation scheme

In the figure above, T_{pmw} is the PWM period, chosen by the user, τ_i is the pulse width in time at each period, and U_{max} is the maximum thrust.

There are two different ways to simulate this behaviour on Simulink: on the one side, in the case of **ideal control** it is necessary to limit the input signal control to the upper and lower saturation value, U_{max} and $-U_{max}$; on the other side, in the case of **real control** a PWPF modulator is added in which the main element is the Schmitt trigger supplemented by a low-pass filter. However, there are entire documents regarding this topic, but it is not the main theme of discussion of this thesis, thus, it will be applied the ideal evaluation just to ensure the thrusters constraints.

1.4.2. Attitude system

For attitude control exists different types of actuators (momentum wheels, thrusters, control moment gyroscopes, etc.), however, **reaction wheels** are the most used devices with this purpose, thanks to their reliability and fast response, even so with the saturation problem [22].

For three-axis control, three reaction wheels are needed mounted along three different directions but usually they are used in clusters of four wheels to guarantee that the system keeps working well in case of failure.

Depending on the geometry of the spacecraft and the functions that it must perform, several configurations are usually proposed. Some of the most used are shown in the figure below.

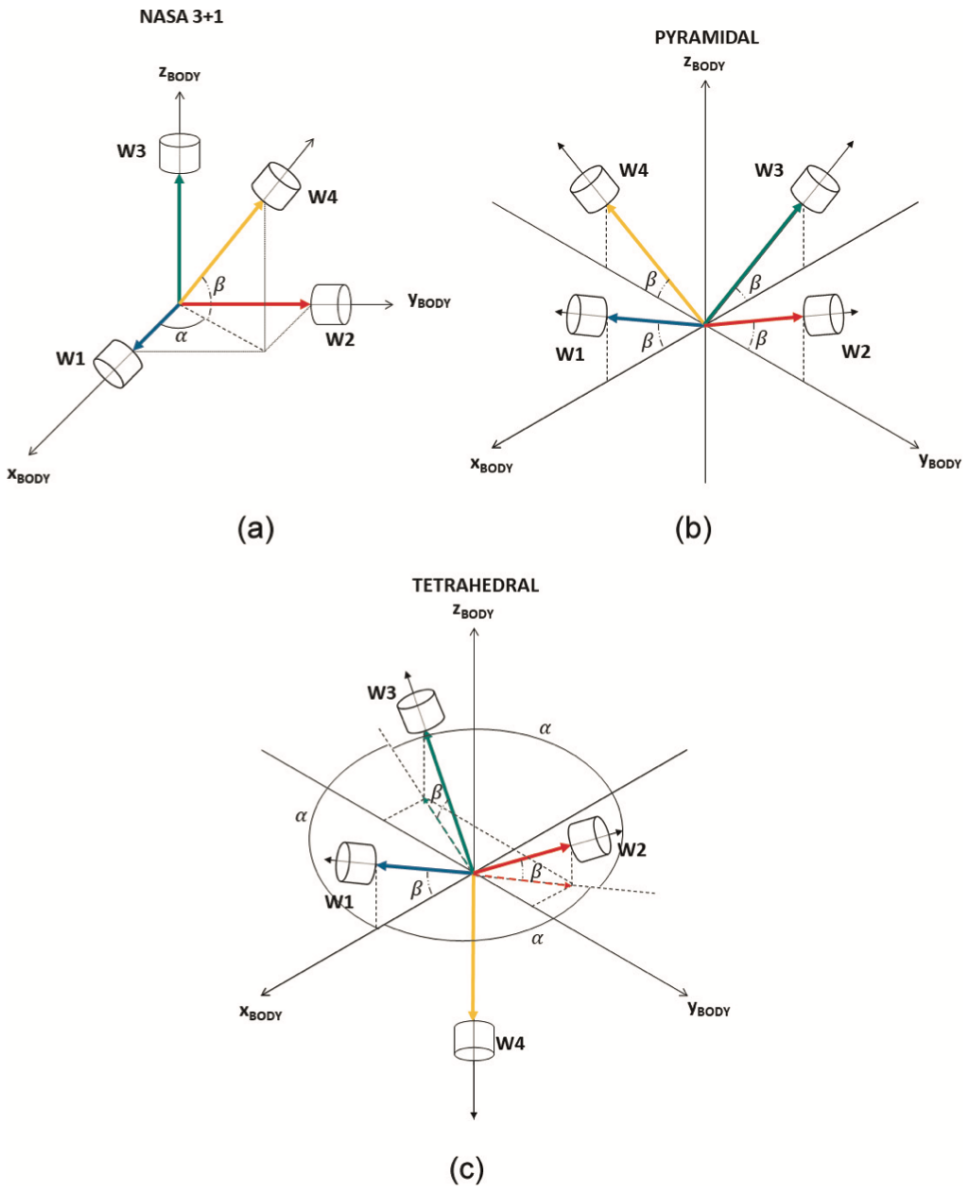

Figure 1.7: NASA 3+1 configuration (a), pyramidal configuration (b), tetrahedral configuration (c) [23]

CHAPTER 2. MISSION DESCRIPTION

2.1. What is space rendezvous?

In a space rendezvous mission a spacecraft has to meet with another one, that is, it must arrive to the same place and at the same time as the second one. Just to understand it in a better way, it can be compared with the case of two basketball players in a counter-attack. In this analogy, the player with the ball has to make the pass at the right time and with the appropriate force so that the ball reaches the moving receiver. Then, the key is the **timing**.

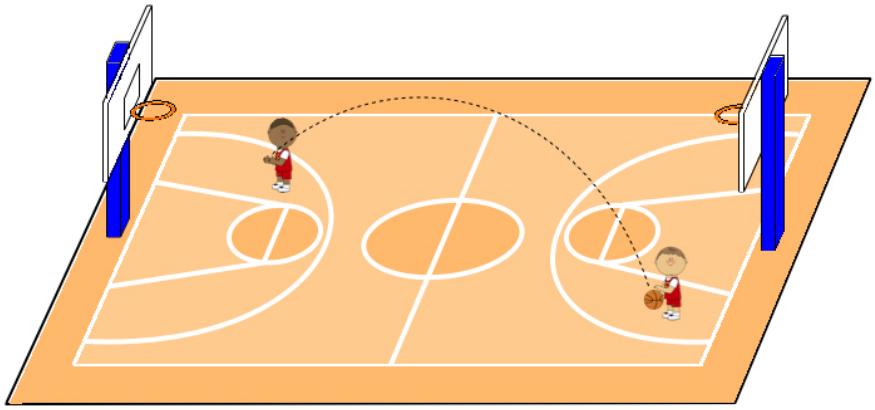

Figure 2.1: Orbital rendezvous and basketball analogy

To analyze this problem let's make some numbers:

$$V_{receiver} = 3\ m/s \qquad ; \qquad V_{ball} = 8\ m/s \qquad ; \qquad d_{pass} = 24\ m$$

The player that makes the pass must 'lead' the receiver, that is, the receiver will travel some distance while the ball is in the air. Then, the time of flight of the ball is defined:

$$TOF_{ball} = d_{pass}/V_{ball} = 3\ s$$

Thus the distance that the receiver will travel while the ball is on the way is:

$$d_{lead} = \text{lead distance} = TOF_{ball} \cdot V_{receiver} = 9\ m$$

This means that the receiver runs an additional 9 m while the ball goes from one point to another. At this point, we can figure out the total head start that the receiver needs before the passer throws the ball:

$$d_{head} = \text{head start distance} = d_{pass} - d_{lead} = 15\ m$$

At that moment, making the assumption that the receiver starts at the same point that passer, before the passer throws the ball the receiver should be 15 m away from him. Then, it can be determined the time that the passer has to wait:

$$WT = \text{waiting time} = d_{head}/V_{receiver} = 5\ s$$

This is the time that the passer must wait before throwing the ball to ensure that the receiver will be at the rendezvous point when the ball arrives.

Going back to the case of a rendezvous between two spacecraft, it will be assumed that both vehicles follow circular orbits and the transfer from one orbit to another will be held by means of a Hohmann transfer orbit. As in the case of the basketball players, the orbital velocity of the interceptor and the target have to be known. However, in space rendezvous these velocities are not linear but rotational (angular velocities), and they can be determined from the orbital radius:

$$\omega = \sqrt{\frac{\mu}{a^3}} \tag{2.1}$$

where μ is the gravitational parameter for Earth and a is the semimajor axis of the orbit. For circular orbits, the semimajor axis is equal to the radius of the orbit, R_{orb}.

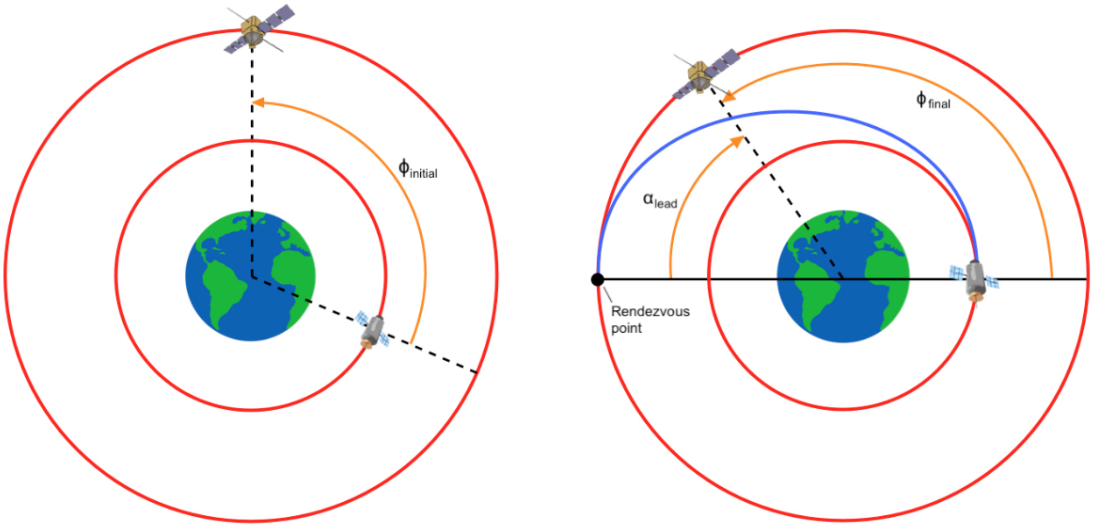

Figure 2.2: Orbital rendezvous [24]

For a rendezvous in orbit, it is also necessary to determine the time of flight of the chaser until it reaches the rendezvous point. As the transfer is done by means of a Hohmann orbit, that corresponds to a half of an elliptical orbit, the time of flight can be computed as:

$$TOF = \pi\sqrt{\frac{a_{transfer}^3}{\mu}} \tag{2.2}$$

As before, the target will cover a certain amount during the time of flight of the chaser spacecraft from the initial orbit to the desired one. Then, once again, the interceptor must lead the target by an angular distance called **lead angle**, α_{lead}, that can be determined multiplying the target's angular velocity by the TOF of the chaser:

$$\alpha_{lead} = \omega_{target} TOF \tag{2.3}$$

At this point, it can be determined the head start that the target spacecraft needs. For spacecraft, it is called **phase angle**, ϕ, and taking into account that during the Hohmann transfer the interceptors travels 180^o, it is computed as:

$$\phi_{final} = \pi - \alpha_{lead} \tag{2.4}$$

Finally, it can be determined the time that the chaser must wait before initiating the rendezvous in order to reach the rendezvous point at the same time that the target:

$$WT = \frac{\phi_{final} - \phi_{initial}}{\omega_{target} - \omega_{chaser}} \tag{2.5}$$

This kind of manoeuvres can be divided, as shown in Figure 2.3, in different major phases:

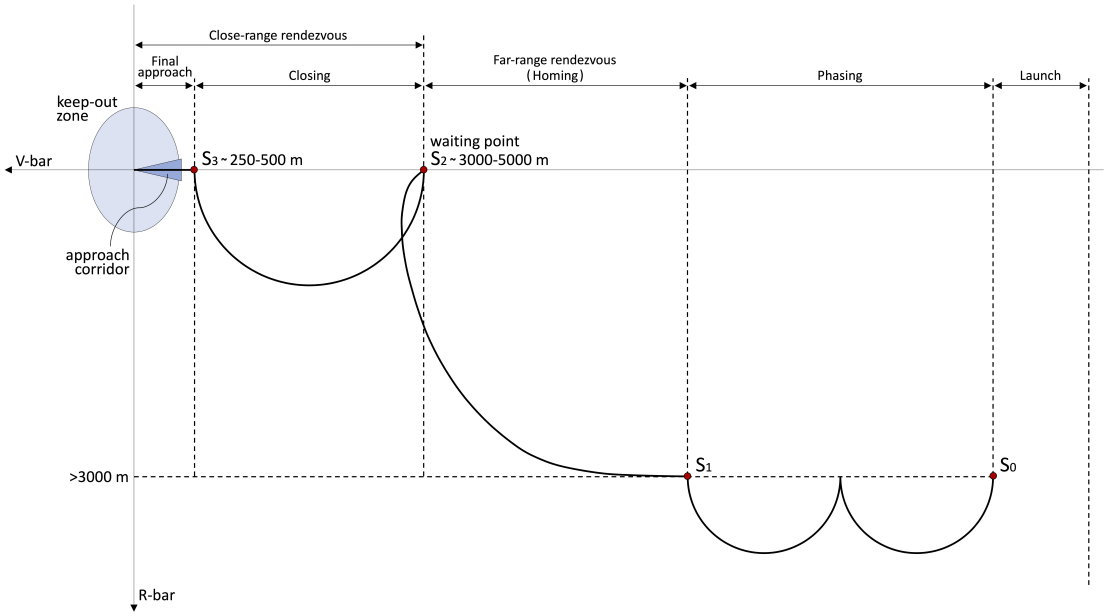

Figure 2.3: Spacecraft rendezvous process [25]

- **Launch.** Injection into the orbital plane of the target and achievement of the stable orbital conditions.
- **Phasing.** The objective is the reduction of the phase angle between chaser and target by taking advantage of the fact that a lower orbit has a higher orbital velocity. Generally, this manoeuvre is controlled from ground and is done by absolute navigation (i.e. ECI reference coordinate system).
- **Far-range rendezvous or homing phase.** The main objective of this phase is to achieve the position, velocity and angular rate conditions necessary to initiate the close range rendezvous operations. Then, in this phase occurs the transfer from the phasing orbit to a new point in close vicinity of the target (i.e. Hohmann transfer). It can start when the relative navigation of the chaser with respect the target is available, that is, the dynamics of the chaser can be measured with respect to the LVLH frame (see section 1.1.2.).
- **Close-range rendezvous.** This phase consists of two smaller phases: in the ***closing phase*** the objectives are the reduction of the chaser-target distance and achievement of the final conditions allowing the acquisition of the final approach corridor; and during the ***final approach***, takes place the approach to the capture point and the achievement of the capture conditions.

Rendezvous may be or may not be followed by **docking** or **berthing**, procedures that bring both spacecraft into physical contact between them.

2.2. Reference satellite

In order to carry out the simulations, the reference spacecraft that has been selected is a 12U CubeSat 1HOPSat (see Figure 2.4) from Hera Systems with the specifications shown in the table below.

Type / Application:	Earth observation
Equipment:	Imaging telescope payload
Configuration:	CubeSat (12U)
Propulsion:	4 electric thrusters
Power:	Deployable fixed solar arrays, batteries
Lifetime:	3-5 years
Mass:	22 kg
Orbit:	LEO

Table 2.1: 12U CubeSat 1HOPSat Specifications

The satellites in this constellation each contain an imaging telescope payload for recording images and video of specified regions of the Earth at 1 meter ground sample distance (GSD).

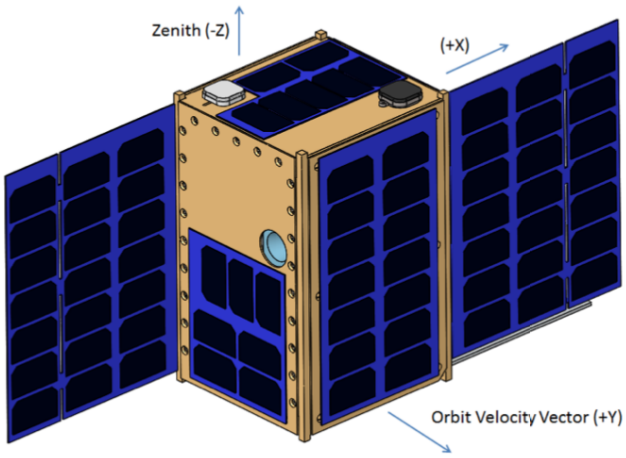

Figure 2.4: 12U CubeSat 1HOPSat model [26]

They consist of a cube-shaped central body of dimensions 0.2x0.34x0.2 m and two deployable solar panels of dimensions 0.2x0.003x0.34 m and an approximated mass of $m_{sp} = 0.2 \cdot 0.34 \cdot 1.76 = 0.1197$ kg. Thereby, the tensor of inertia of the whole satellite, taking into account the uncertainty due to the solar panels extension, can be computed as follows:

$$J_{SC} = J_0 + \Delta J \tag{2.6}$$

where J_0 is the nominal tensor of inertia of the spacecraft and ΔJ the variation added to the nominal tensor. Both components can be computed as:

$$J_0 = \begin{bmatrix} m_c(l_y^2 + l_z^2)/12 & 0 & 0 \\ 0 & m_c(l_x^2 + l_z^2)/12 & 0 \\ 0 & 0 & m_c(l_x^2 + l_{y_{sp}}^2)/12 \end{bmatrix} \tag{2.7}$$

$$\Delta J = \begin{bmatrix} m_{sp}(l_{y_{sp}}^2 + l_z^2)/12 & 0 & 0 \\ 0 & m_{sp}(l_x^2 + l_z^2)/12 & 0 \\ 0 & 0 & m_{sp}(l_x^2 + l_y^2)/12 \end{bmatrix} \tag{2.8}$$

Then, the total tensor of inertia of the chaser spacecraft is equal to:

$$J_0 = \begin{bmatrix} 0.2900 & 0 & 0 \\ 0 & 0.2980 & 0 \\ 0 & 0 & 0.1570 \end{bmatrix} [kgm^2]$$

2.2.1. Propulsion system

Instead of considering the original propulsion system of the satellite, a different configuration as the one illustrated in Figure 2.5 is proposed. It is composed of 12 thrusters able to provide a maximum force of $F_{max} = 0.5$ N each one in the direction in which are orientated.

Considering an ideal working system, the main advantage of this scheme is that thrusters are disposed so that the torques introduced due to the deviation from the center of gravity of the satellite are canceled between them. Moreover, it is a redundant configuration since if one of the thrusters fails, there is another one that may continue providing a force in the same direction. In case this situation happened, the moment exerted on the spacecraft should be compensated by the ACS.

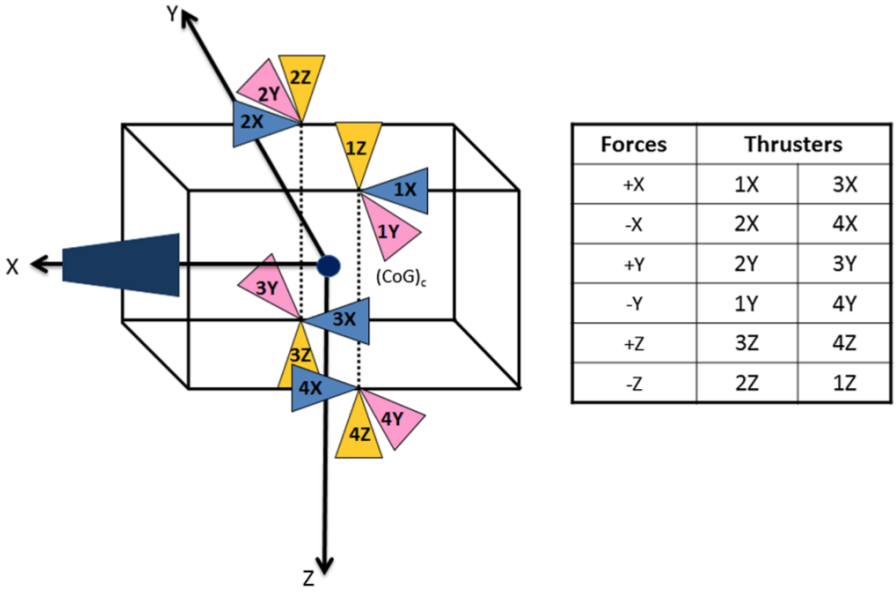

Forces	Thrusters	
+X	1X	3X
-X	2X	4X
+Y	2Y	3Y
-Y	1Y	4Y
+Z	3Z	4Z
-Z	2Z	1Z

Figure 2.5: Thruster scheme on the spacecraft [27]

2.2.2. Attitude Control System

For the reaction wheels system, it has been chosen a classical configuration commonly used in this kind of satellites. It consists in a cluster of 4 reaction wheels in a square pyramid configuration, as shown in Figure 2.6. Each wheel is properly arranged with an inclination with respect to the horizontal plane of $\beta = 45^o$. This configuration allows to maximize torques in all directions, minimizing torque cancellations between wheels, and provides redundancy in the case of a reaction wheel failure [28]. The exploited arrangement of the wheels is $\alpha_1 = 0^o$, $\alpha_2 = 90^o$, $\alpha_3 = 180^o$ and $\alpha_4 = 270^o$.

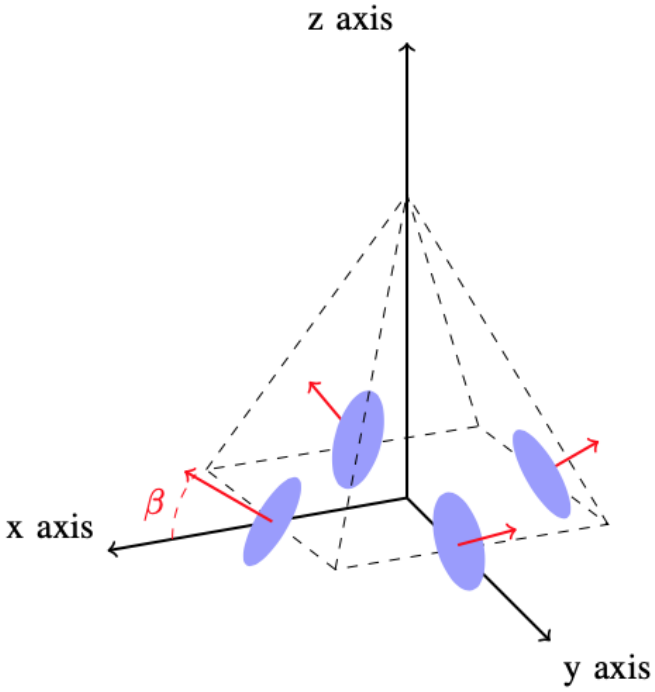

Figure 2.6: Configuration of the reaction wheel system: Square pyramid [29]

Each of the reaction wheels is able to provide a maximum torque equal to $M_{max} = 0.025$ Nm with respect to its local frame, that must be expressed in the body frame of the spacecraft (see section 1.1.3.).

At this point, in order to evaluate the total angular momentum introduced by each reaction wheel, w_i, in the body frame starting from the wheel frame, the following transformation matrix must be applied:

$$ {}^{B}\mathrm{R}^{W_i} = \begin{bmatrix} \cos\alpha_i \cos\beta & -\sin\alpha_i & \cos\alpha_i \sin\beta \\ \sin\alpha_i \cos\beta & \cos\alpha_i & \sin\alpha_i \sin\beta \\ -\sin\beta & 0 & \cos\beta \end{bmatrix} \tag{2.9} $$

Thus, the total angular momentum in the inertial frame can be computed by summing all the angular momentum of the wheels, $h_{w_i}^{W_i}$, represented in the body frame, $h_{w_i}^{B}$:

$$ h_w^B = \sum_{i=1}^{4} {}^{B}\mathrm{R}^{W_i} h_{w_i}^{W_i} \tag{2.10} $$

And evaluated, independently, on each axis becomes:

$$h_x = h_1 \cos\alpha_1 \sin\beta + h_2 \cos\alpha_2 \sin\beta + h_3 \cos\alpha_3 \sin\beta + h_4 \cos\alpha_4 \sin\beta \tag{2.11}$$

$$h_y = h_1 \sin\alpha_1 \sin\beta + h_2 \sin\alpha_2 \sin\beta + h_3 \sin\alpha_3 \sin\beta + h_4 \sin\alpha_4 \sin\beta \tag{2.12}$$

$$h_z = h_1 \cos\beta + h_2 \cos\beta + h_3 \cos\beta + h_4 \cos\beta \tag{2.13}$$

Finally, just to express it with a shorter notation, the total angular momentum can be written as the product between the matrix P and the vector h_w^W as follows:

$$h_w^B = \sum_{i=1}^{4} {}^B\mathrm{R}^{W_i} h_{w_i}^{W_i} = P h_w^W \tag{2.14}$$

where

$$h_w^W = [h_1, h_2, h_3, h_4]^T \tag{2.15}$$

and

$$P = \begin{bmatrix} c\alpha_1 s\beta & c\alpha_2 s\beta & c\alpha_3 s\beta & c\alpha_4 s\beta \\ s\alpha_1 s\beta & s\alpha_2 s\beta & s\alpha_3 s\beta & s\alpha_4 s\beta \\ c\beta & c\beta & c\beta & c\beta \end{bmatrix} \tag{2.16}$$

With the arrangement described above, $\beta = 45^o$ and $\alpha_1 = 0^o$, $\alpha_2 = 90^o$, $\alpha_3 = 180^o$ and $\alpha_4 = 270^o$, the transformation matrix is equal to:

$$P = \begin{bmatrix} \frac{\sqrt{2}}{2} & 0 & -\frac{\sqrt{2}}{2} & 0 \\ 0 & \frac{\sqrt{2}}{2} & 0 & -\frac{\sqrt{2}}{2} \\ \frac{\sqrt{2}}{2} & \frac{\sqrt{2}}{2} & \frac{\sqrt{2}}{2} & \frac{\sqrt{2}}{2} \end{bmatrix} \tag{2.17}$$

Since the reaction wheels have a maximum working angular velocity, that is, a maximum torque, as explained in section 1.4., they are saturated to the lower and upper saturation value, $-M_{max}$ and M_{max}. As will be seen later, the control algorithms provide the necessary torque commands with respect to the body frame, and then, it will be needed to find from Eq. 2.14 the moment introduced by each wheel. Although it seems simple matrix calculations, matrix P is not square and it is not possible to compute its inverse, P^{-1}, so a mathematical concept known as **Moore-Penrose pseudoinverse** must be introduced:

$$P^+ = (P^T P)^{-1} P^T \tag{2.18}$$

CHAPTER 3. GUIDANCE, NAVIGATION AND CONTROL

On the onboard rendezvous control system of spacecraft, one of the main subsystems is the Guidance, Navigation and Control system. The GNC system deals with the control of the movement of space vehicles, both translational and rotational dynamics, and a block diagram of a typical control loop is shown in Figure 3.1.

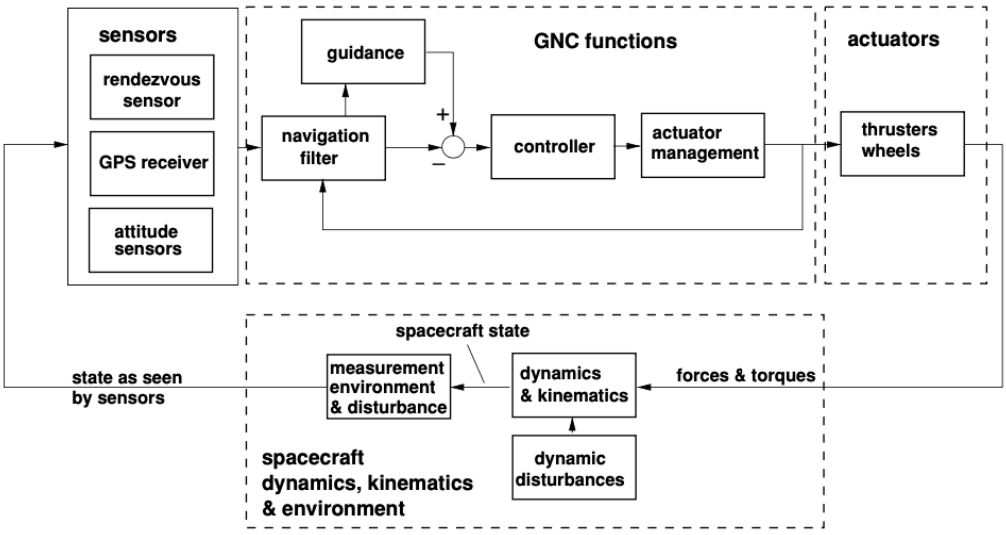

Figure 3.1: GNC functions [12]

On the one side, the **guidance function** defines the trajectory that the spacecraft has to follow to reach the desired final position, as well as the changes in velocity, rotation and acceleration needed to follow that path.

On the other side, the **navigation function** tries to find the present and the future position using the measures provided by the sensors. It consists of a Kalman filter that processes the various information of attitude and trajectory sensors and propagates the vehicle state in position and attitude by using the knowledge of the dynamic behaviour and information on the current thrust commands.

Finally, the objective of the **control function** is to provide the force and torque commands that will execute the Reaction Control System (RCS) and the Attitude Control System (ACS) to match the current state with the desired state.

3.1. Guidance algorithms

Guidance algorithms may be classified in three classes:

1. **Predictive Feedback Guidance Laws:** in these kind of algorithms, the behaviour of the target is supposed to be known, then it is possible to know the position of the target at any time. This class includes algorithms as Lambert guidance and Time-Varying State Transition Matrix (STM) guidance.

2. **Feedback-based Guidance Laws:** the working of these type of algorithms consists in the measurement of the actual dynamics to do the proper corrections to reach the desired position. Among the algorithms in this class, there are laws such as Proportional Navigation (PN) guidance, ZEM/ZEV guidance or Pulsed PN (PPN) guidance.

3. **Optimal Feedback Guidance Algorithms:** for some applications, it is desirable to specify terminal conditions. In this kind of operations, the main goal is to go from an initial position to a desired one, however, sometimes there may be terminal velocity requirements. Three different optimal guidance laws are considered: Constrained Terminal Velocity Guidance (CTVG), in which the terminal velocity is constrained in magnitude and direction; Free Terminal Velocity Guidance (FTVG), in which only the direction of the terminal velocity is constrained; or Intercept Angle Control Guidance (IACG), when it is wanted the chaser to approach the target with a determined angle.

In this thesis, two of the proposed guidance algorithms are analyzed, a **PN guidance** and **CTVG algorithm**. As shown in the following sections, both guidance laws already provide as an output an acceleration command, thus, these guidance algortihms, as by definition, include a feedback loop, in order to directly assign the command input to the RCS.

3.1.1. Proportional Navigation Guidance

Proportional Navigation is one of the earliest feedback guidance laws. Its origins date back to the middle of the 20th century, during World War II, with the first **tactical missiles** [30]. However, it wasn't until 1956 when this homing missile technique was applied directly in space rendezvous operations by Walter Wrigley, with the assumptions that this entailed: constant relative velocity and small lead angle. Then, more than 10 years later came a first approach in optimization of proportional navigation.

In the beginning, this automatic trajectory control technique was applied successfully in aeronautical interception problems, in which only the position of both target and seeker were to be matched. Nowadays, the homing missile manoeuvre is just a special class of proportional navigation in which the condition of constant relative velocity mentioned above is just an additional constraint and, thus, a velocity end condition is introduced since in space rendezvous missions also the velocity of both vehicles are to be matched (reduce relative velocity to zero) [31].

The PN guidance law computes acceleration commands perpendicular to the instantaneous line-of-sight (LOS) direction, the target-chaser connection line, attempting to drive the LOS rate to zero. The PN guidance law is expressed as:

$$a = nV_c\dot{\lambda} \tag{3.1}$$

Then, decomposing this acceleration command in the components of the XZ plane in LVLH frame described in section 1.1.2., it becomes [32, 33]:

$$a_x = -nV_c\dot{\lambda}\sin\lambda \tag{3.2}$$

$$a_z = nV_c\dot{\lambda}\cos\lambda \tag{3.3}$$

where λ is the LOS angle, $\dot{\lambda}$ is the LOS rate, V_c is closing velocity with respect to the target, and n is the effective navigation ratio, typically chosen between 3 and 5. Larger values are set to provide more robustness against disturbances and errors, nevertheless, they also may cause unnecessary large accelerations; instead, small values of the navigation ratio may command too little accelerations and then miss the target. These terms can be evaluated as:

$$\lambda = \arctan\frac{x}{z} \tag{3.4}$$

$$\dot{\lambda} = -\frac{(x\dot{z} - z\dot{x})}{r^2} \tag{3.5}$$

$$V_c = -\dot{r} = -\frac{(x\dot{x} - z\dot{z})}{r} \tag{3.6}$$

with x and z the position of the chaser with respect to LVLH frame, $\dot{x}$ and $\dot{z}$ the velocities and $r = \sqrt{x^2 + z^2}$ the target-chaser distance.

These kind of guidance law uses a predefined trajectory as a reference to compute the acceleration commands that should be applied at any time in order to achieve the final desired position. Then, the more points of the ideal trajectory are known, the smaller the final error in the final position.

3.1.2. Constrained Terminal Velocity Guidance

Mainly, optimal guidance algorithms are investigated for planetary and asteroid proximity operations, including asteroid rendezvous, soft landing, intercept and intercept with impact angle control. Then, for this kind of applications the terminal velocity may have direction and magnitude requirements, and this, as indicated above, is the purpose of the CTVG law. Considering an optimal control problem for minimizing the integral of the acceleration commands squared with the following **performance index**:

$$J = \frac{1}{2}\int_{t_0}^{t_f} \mathbf{a}^T \mathbf{a}\, \mathrm{d}t \tag{3.7}$$

It can be demonstrated from the Hamiltonian and the costate equations that the optimal control acceleration to compute the acceleration commands that minimize the performance index above is found as [33, 34]:

$$\mathbf{a} = \frac{6[\mathbf{r}_f - (\mathbf{r} + t_{go}\mathbf{v})]}{t_{go}^2} - \frac{2(\mathbf{v}_f - \mathbf{v})}{t_{go}} - \mathbf{g} \tag{3.8}$$

or

$$\mathbf{a} = \frac{6[\mathbf{r}_f - (\mathbf{r} + t_{go}\mathbf{v}_f)]}{t_{go}^2} + \frac{4(\mathbf{v}_f - \mathbf{v})}{t_{go}} - \mathbf{g} \tag{3.9}$$

where $\mathbf{r}$, $\mathbf{r}_f$, $\mathbf{v}$ and $\mathbf{v}_f$ are the actual and final position and velocity vectors, respectively, $\mathbf{g}$ is the gravity acceleration assumed to be constant here, and $t_{go} = t_f - t_0$ is the time-to-go from the initial to the desired position.

In the case of soft landing, it is desired to have zero final velocity, $\mathbf{v}_f = 0$. This can be directly extrapolated to the case of a rendezvous mission between two spacecraft, in which

is desired to have at the end of the manoeuvre a relative velocity between both vehicles equal to zero. Thus, taking into account this constraint, Eqs. 3.8 and 3.9 become:

$$\mathbf{a} = \frac{6(\mathbf{r}_f - \mathbf{r})}{t_{go}^2} + \frac{2\mathbf{v}}{t_{go}} - \mathbf{g} \tag{3.10}$$

and

$$\mathbf{a} = \frac{6(\mathbf{r}_f - \mathbf{r})}{t_{go}^2} - \frac{4\mathbf{v}}{t_{go}} - \mathbf{g} \tag{3.11}$$

In contrast of PN guidance, this guidance laws use a **specified time-to-go** as an input parameter, that is, a predefined time to travel from the initial position to the desired one, and compute the acceleration needed to reach the target at a final time as close as possible to the predetermined one. Then, assuming that **g** is negligible, it is possible to demonstrate that the value of time-to-go that minimizes the performance index from Eq. 3.7 becomes:

$$t_{go} = \begin{cases} \tau & ; B^2 - 4AC > 0 \text{ and } B > 0 \\ \text{no solution; otherwise} \end{cases} \tag{3.12}$$

where

$$\tau = \frac{-B - \sqrt{B^2 - 4AC}}{2A} \tag{3.13}$$

$$A = (\mathbf{v}^T\mathbf{v} + \mathbf{v}_f^T\mathbf{v} + \mathbf{v}_f^T\mathbf{v}_f) \geqslant 0 \tag{3.14}$$

$$B = 6(\mathbf{r}_f - \mathbf{r})^T(\mathbf{v}_f + \mathbf{v}) \tag{3.15}$$

$$C = 9(\mathbf{r}_f - \mathbf{r})^T(\mathbf{r}_f - \mathbf{r}) \tag{3.16}$$

Sometimes, because of the initial and the imposed final conditions, it may happen that there is no possible solution, and then, increasing t_{go} leads to decreasing the performance index.

3.2. Control algorithms

As previously stated, for the guidance algorithms that are studied in this thesis it is no necessary the use of a control algorithm for translational dynamics. Nevertheless, the control of rotational dynamics, that is, the attitude of the spacecraft, has also the same degree of importance, so well designing a controller able to lead the initial attitude of the spacecraft to the desired position in a stable way, avoiding oscillations and in a reasonable amount of time is a really important task.

There are several kind of control techniques that can deal with this work: LQR (Linear Quadratic Regulator), MPC (Model Predictive Control), H_∞ Output-Feedback, Sliding Mode Control (SMC), etc. In this thesis, for the control of the attitude of the spacecraft a simple scheme using **linear quaternion feedback control** is implemented with the usw of a **PD** (Proportional-Derivative) **control** scheme.

3.2.1. PD controller

A **PID** (Proportional-Integral-Derivative) **controller** is a control loop mechanism utilizing feedback that use the three control terms of **proportional, integral and derivative** influence on the controller output to apply accurate and optimal control. This kind of controllers are one of simplest and are adjusted empirically.

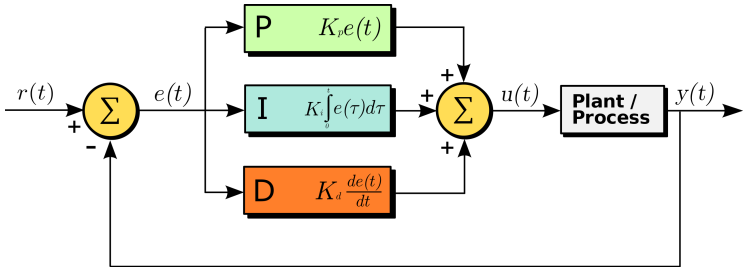

Figure 3.2: Block diagram of a PID controller in a feedback loop

From Figure 3.2, the closed-loop transfer function of the PID controller is:

$$PID(s) = \frac{u(s)}{e(s)} = K_p + K_i \frac{1}{s} + K_d s \tag{3.17}$$

where K_p, K_i and K_d are the proportional, integrative and derivative parameters, respectively. When choosing the value of these control terms, the minimum requirements of the system must be considered. The following table shows the effects of increasing a parameter independently:

	Rise time	Overshoot	Settling time	Steady-state error	Stability
K_p	decrease	increase	small increase	decrease	decrease
K_i	small decrease	increase	increase	large decrease	decrease
K_d	small decrease	decrease	decrease	minor change	increase

Table 3.1: Effects of increasing a parameter from the PID controller

This kind of controllers were initially implemented in electronic devices and were tuned using a trial and error method. They were implemented for the first time in aerospace industry in 1930's and, nowadays, most of the aerospace industrial applications continue to be operated by PID controllers.

As has been said above, in this case a **PD controller** is used, which means that the integrative term is set to zero. Then, the commanded control torques for the reaction wheels of the attitude control system can be computed as:

$$\mathbf{M}_{RW} = \begin{bmatrix} \mathbf{K}_p & \mathbf{K}_d \end{bmatrix} \begin{bmatrix} \mathbf{q}_{err} \\ \boldsymbol{\omega} \end{bmatrix} = \mathbf{K}_p \mathbf{q}_{err} + \mathbf{K}_d \boldsymbol{\omega} \tag{3.18}$$

$$\mathbf{K}_p = \begin{bmatrix} K_{p_x} & 0 & 0 \\ 0 & K_{p_y} & 0 \\ 0 & 0 & K_{p_z} \end{bmatrix} \tag{3.19}$$

$$\mathbf{K}_p = \begin{bmatrix} K_{dx} & 0 & 0 \\ 0 & K_{dy} & 0 \\ 0 & 0 & K_{dz} \end{bmatrix} \tag{3.20}$$

where $\mathbf{q}_{err} \in \mathbb{R}^3$ is the attitude quaternion error, $\boldsymbol{\omega} \in \mathbb{R}^3$ is the body angular rate of the spacecraft and $\mathbf{K}_p$, $\mathbf{K}_d \in \mathbb{R}^{3\times3}$ are the proportional and derivative terms of the controller, respectively.

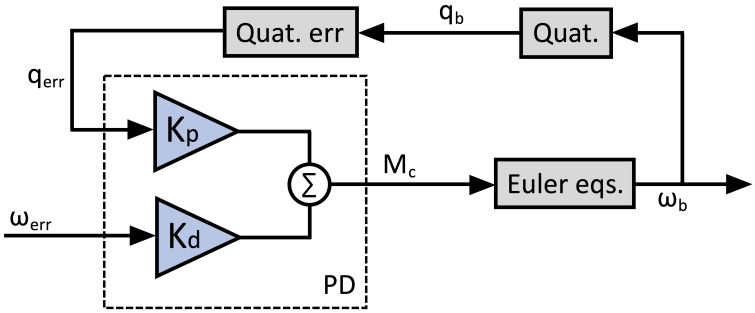

Figure 3.3: Block diagram of the PD controller

All three control channels, $[x, y, z]^T$, can be tuned independently as SISO (Single Input Single Output) systems.

CHAPTER 4. SIMULATIONS AND RESULTS

This chapter shows the results of the simulations of the two proposed scenarios explained below. The objective of these simulations is to evaluate the efficiency of the designed control system and the effectiveness of the proposed guidance and control algorithms.

Moreover, regarding the PN algorithm defined in the section 3.1.1., in this research two different configurations of this law will be tested, as illustrated in Figure 4.1: in the first one the acceleration commands are computed considering both position and velocity of the reference trajectory, in the second configuration it is also considered the velocity of the reference trajectory but the real position of the chaser in order to have a feedback of its current state.

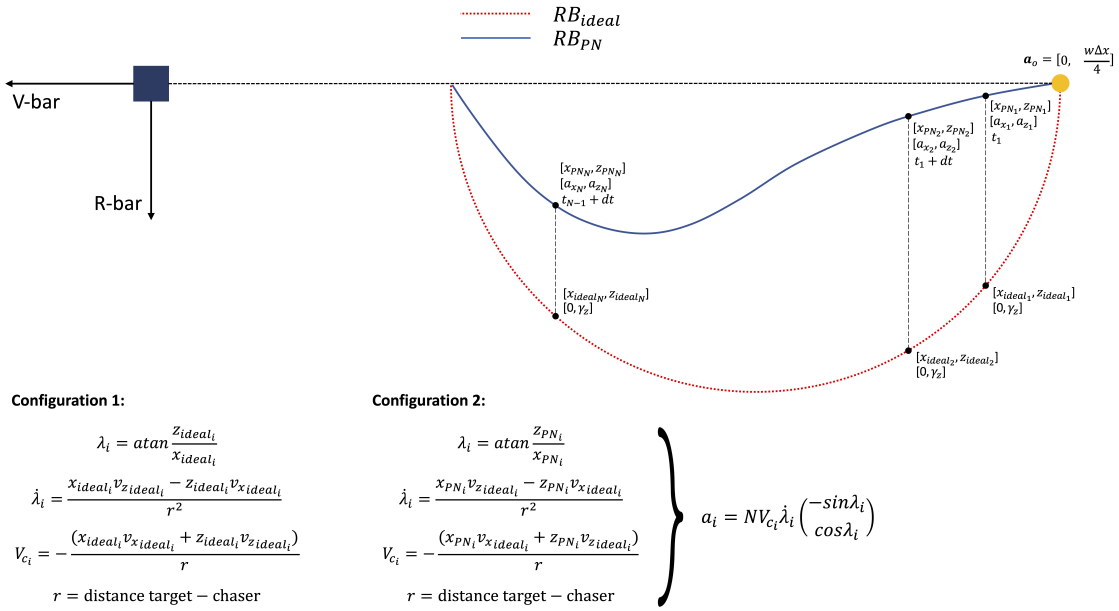

Figure 4.1: Proportional Navigation guidance scheme for rendezvous

4.1. Mission scenarios

Mainly, the reference satellite proposed in this thesis are used for **Earth observation missions**, in which the key role is demanded to the attitude control, and **debris capture missions**, in which the working of the orbital control is one of the most important parts. Thus, in order to compare the operating mode of both guidance algorithm and control algorithm studied in this thesis (see Chapter 3), two different scenarios are presented: **Crab Nebula observation** and **Debris closing and observation** [22].

4.1.1. Crab Nebula observation

The main goal of this mission is to observe the Crab Nebula. It is assumed that the satellite already starts at the final orbit, then, the scenario consists of two pointing manoeuvres:

in the first one the satellite has to point towards the Crab Nebula, thus it must align to the desired quaternion $\mathbf{q}_{des} = [0.9214, 0.1029, 0.0416, 0.3725]^T$ with null angular velocity $\omega_{des} = [0, 0, 0]^T$ rad/s. For this manoeuvre the initial conditions are:

- **Initial attitude:** $\mathbf{q}_{ini} = [0.7886, 0.2343, 0.5180, 0.2343]^T$
- **Initial angular velocity:** $\omega_{ini} = [0.05, 0.05, 0.05]^T$ rad/s

It is assumed that after 650 s from the beginning of the simulation the satellite has collected all the needed data, and then, the second manoeuvre takes place in which the spacecraft must point to the Earth, that is it has to align to the ideal quaternion $\mathbf{q}_{id} = [1, 0, 0, 0]^T$, to send the data to a ground station, also with null angular velocity.

Figure 4.2: Crab Nebula. Source: NASA, 2017

4.1.2. Debris closing and observation

In this mission scenario, the satellite starts at the debris' orbit, that is located at an altitude $h = 500$ km above the sea level. Then, it must carry out the closing phase performing three radial boosts manoeuvres along V-bar in order to get closer to the target, keeping the relative velocity null after each manoeuvre:

- **1st radial boost:** $C_1 = [-3000, 0, 0]^T$ m $\longrightarrow C_2 = [-500, 0, 0]^T$ m.
- **2nd radial boost:** $C_2 = [-500, 0, 0]^T$ m $\longrightarrow C_3 = [-200, 0, 0]^T$ m.
- **3rd radial boost:** $C_3 = [-200, 0, 0]^T$ m $\longrightarrow C_4 = [-50, 0, 0]^T$ m.

During the first radial boost, the attitude control system of the chaser has to reach the desired quaternion $\mathbf{q}_{des} = [0.8365, -0.1294, 0.2241, 0.4830]^T$ and keep it until the end of the closing. For this manoeuvre the initial conditions are:

- **Initial attitude:** $\mathbf{q}_{ini} = [0.5, 0.5, 0.5, 0.5]^T$
- **Initial angular velocity:** $\omega_{ini} = [0.05, 0.05, 0.05]^T$ rad/s

From this point would start the final approach phase of the rendezvous process, in which the satellite would get close enough from the target to capture it, however, the simulations will stop at this point.

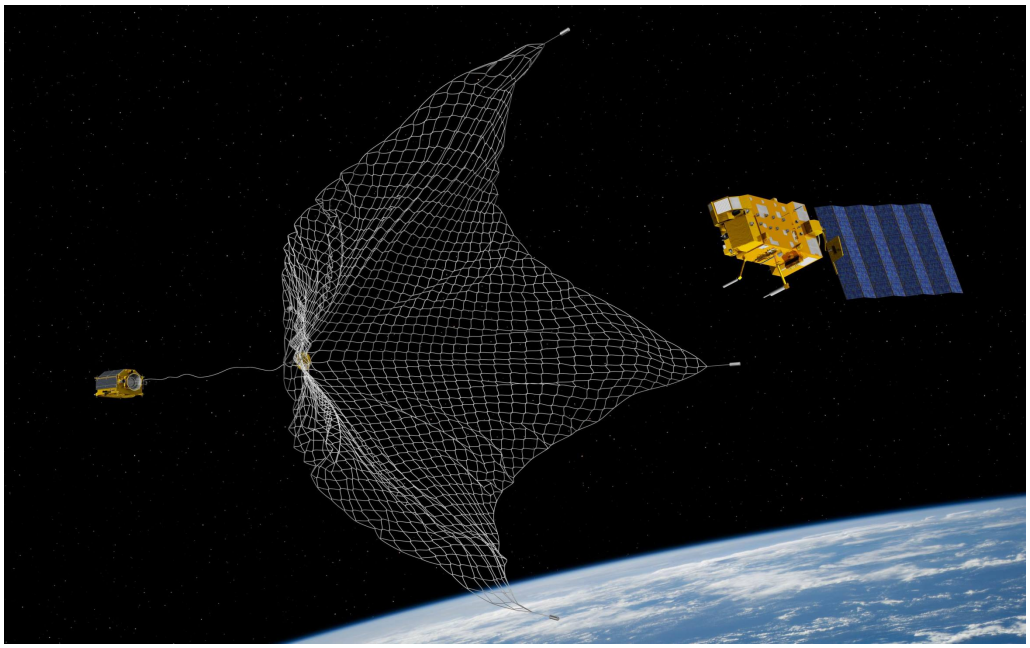

Figure 4.3: e.Deorbit; capture a derelict satellite. Source: ESA, 2016

4.2. Crab Nebula observation results

The numerical results of the Crab Nebula observation mission are shown in the following tables: Table 4.1 shows the results of the first manoeuvre and Table 4.2 those of the second manoeuvre.

	Manoeuvre 1			
	q_0	q_1	q_2	q_3
$\mathbf{q}_{des}$	0.9214	0.1029	0.0416	0.3725
$\mathbf{q}_f$	0.921379	0.102897	0.041601	0.372491
$\mathbf{q}_{err}$	0.999977	-1.773418·10^{-11}	1.596975·10^{-6}	-3.359713·10^{-7}
	ϕ	θ	ψ	
$[\phi,\theta,\psi]_{err}$	-3.654162·10^{-11}	3.193881·10^{-6}	-6.719582·10^{-7}	
	ω_x	ω_y	ω_z	
ω_f	-1.086062·10^{-15}	6.206852·10^{-17}	-2.425071·10^{-15}	

Table 4.1: Manoeuvre 1 - Final attitude and angular rate. All values are given in ISU

	Manoeuvre 2			
	q_0	q_1	q_2	q_3
$\mathbf{q}_{des}$	1	0	0	0
$\mathbf{q}_f$	1.000004	1.048832·10^{-12}	9.097783·10^{-14}	-3.675961·10^{-7}
$\mathbf{q}_{err}$	1.000004	1.048832·10^{-12}	9.097783·10^{-14}	-3.675961·10^{-7}
	ϕ	θ	ψ	
$[\phi,\theta,\psi]_{err}$	2.097656·10^{-12}	1.819571·10^{-13}	-7.351897·10^{-7}	
	ω_x	ω_y	ω_z	
ω_f	5.222723·10^{-13}	-3.893436·10^{-13}	2.754747·10^{-13}	

Table 4.2: Manoeuvre 2 - Final attitude and angular rate. All values are given in ISU

It can be observed from the tables below that in both manoeuvres the spacecraft has reached the desired attitude. In both phases, as can be observed in Figures 4.4-4.9, the system has some oscillations until about 100 s after the start of the manoeuvre and 50 s they have disappeared at all. Then, the attitude control system needs about 150 s to reach the final attitude.

In both operations, Manoeuvre 1 and Manoeuvre 2, it can be considered that at the end of each manoeuvre the satellite is pointing to a fixed point since the angular rates of the spacecrafts have a magnitude of 10^{-15} rad/s and 10^{-13} rad/s, respectively, thus it has practically stopped at all. Also, at the end of Manoeuvre 1 the final attitude has a maximum deviation in radians of about 10^{-6} in the y-axis, that corresponds to a precision of $\pm 0.0002^{o}$. On the other side, when being about to reach the ideal quaternion in Manoeuvre 2, the pointing precision in the x-axis and y-axis has increased considerable, thus system has achieved the desired attitude with a precision of $\pm 0.00005^{o}$.

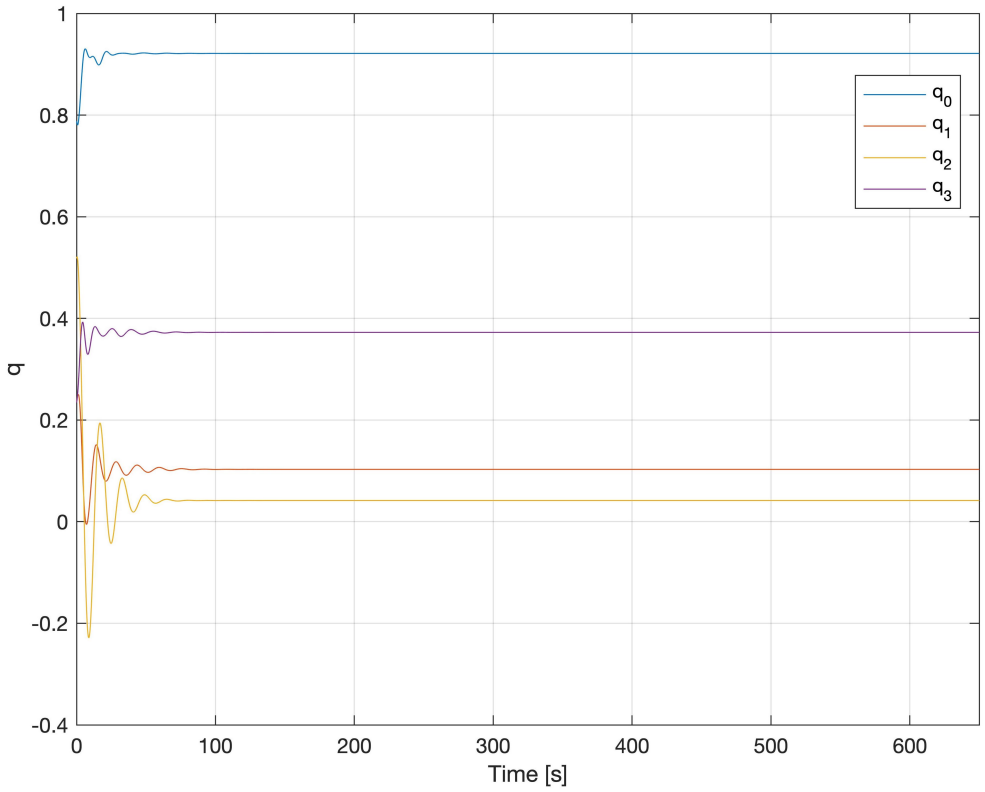

Figure 4.4: Quaternions in time - Manoeuvre 1

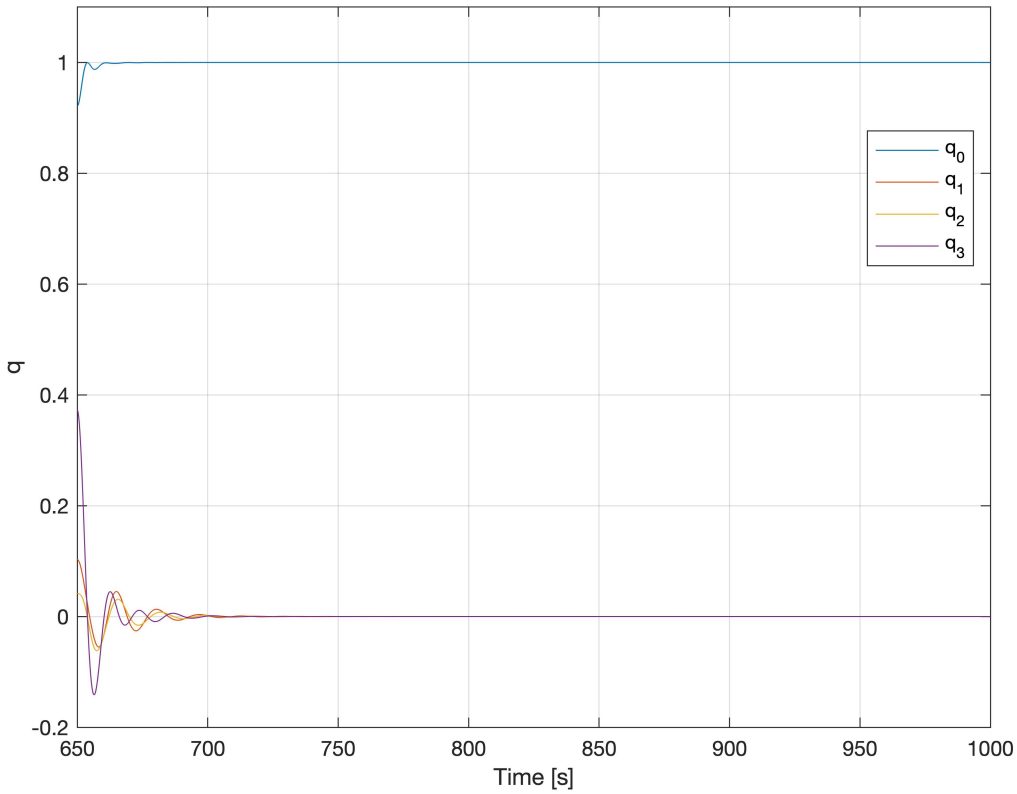

Figure 4.5: Quaternions in time - Manoeuvre 2

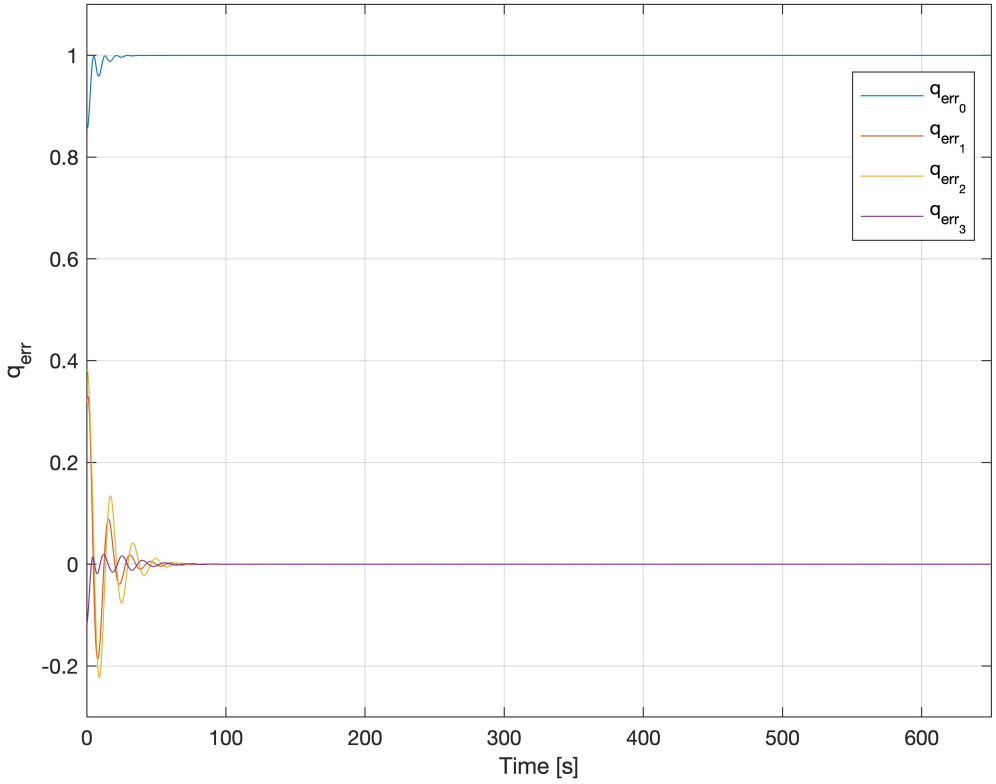

Figure 4.6: Quaternions error in time - Manoeuvre 1

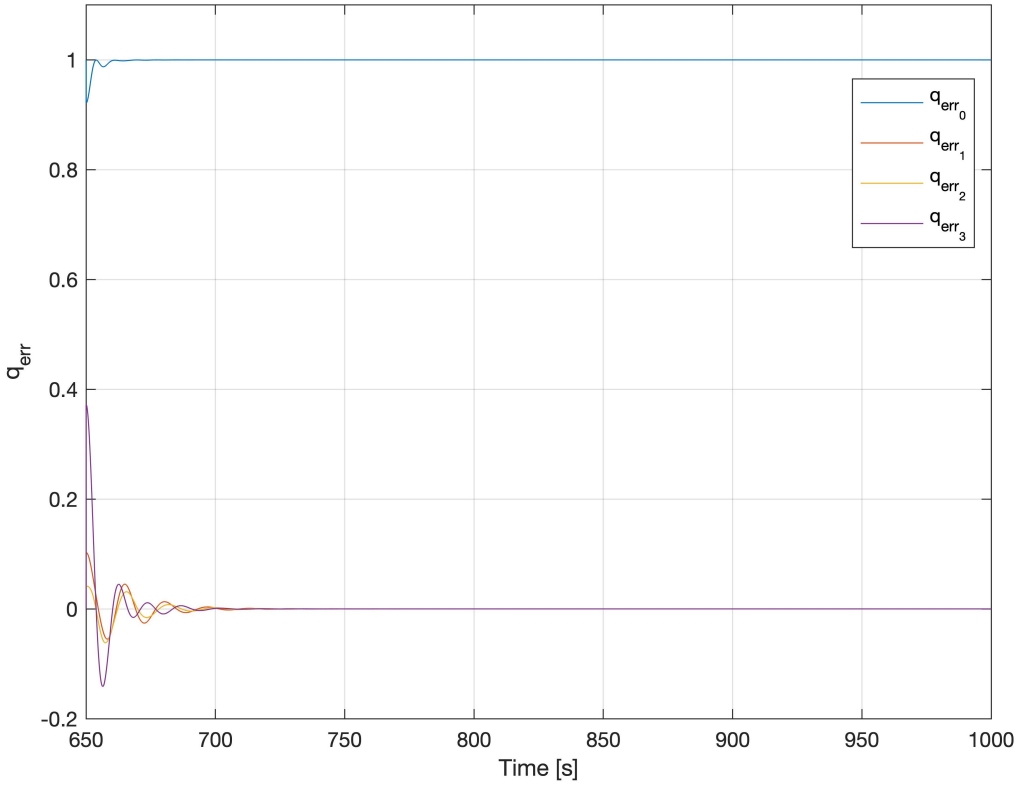

Figure 4.7: Quaternions error in time - Manoeuvre 2

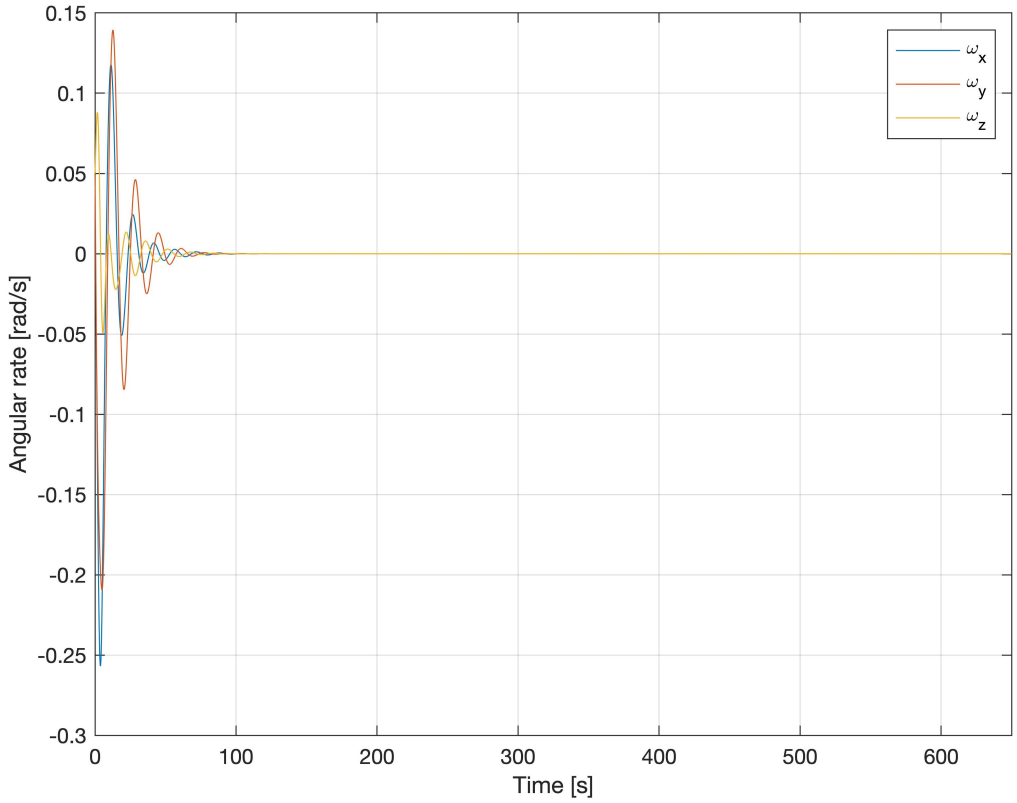

Figure 4.8: Angular rate in time of the spacecraft - Manoeuvre 1

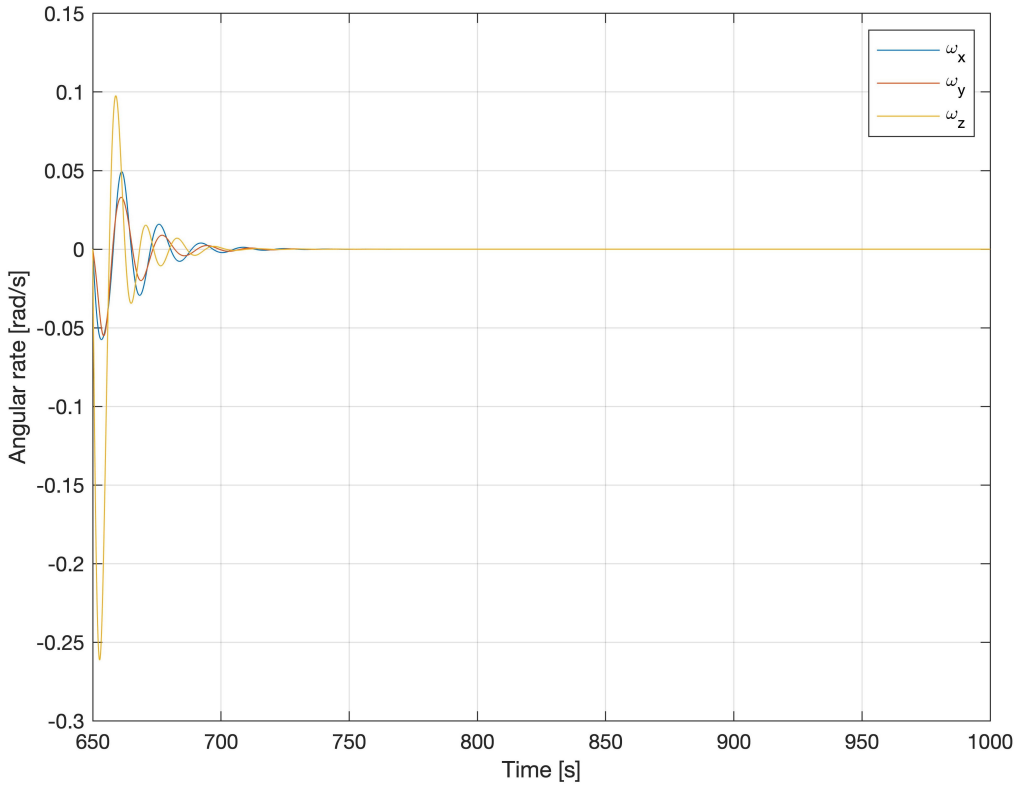

Figure 4.9: Angular rate in time of the spacecraft - Manoeuvre 2

It can be observed in Figure 4.10 that during the firsts moments of the simulation the torque commanded by the controller to the reaction wheel 4 surpasses the maximum torque that it can provide. However, as illustrated in Figure 4.12 it has been saturated to the upper limit and it has not supposed a problem when trying to get the desired attitude.

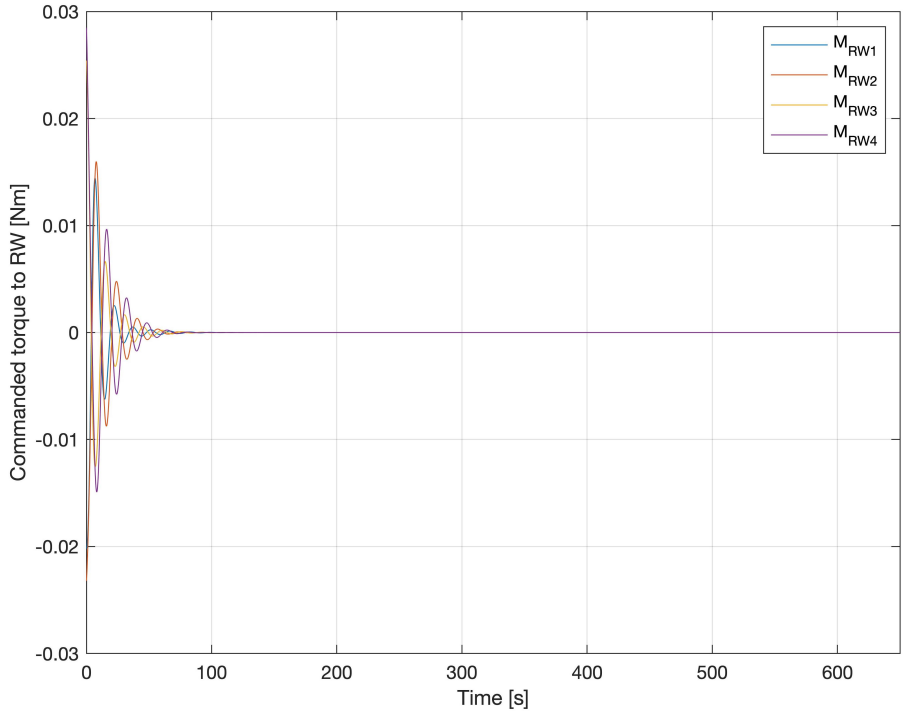

Figure 4.10: Torque commanded to the reaction wheels in time - Manoeuvre 1

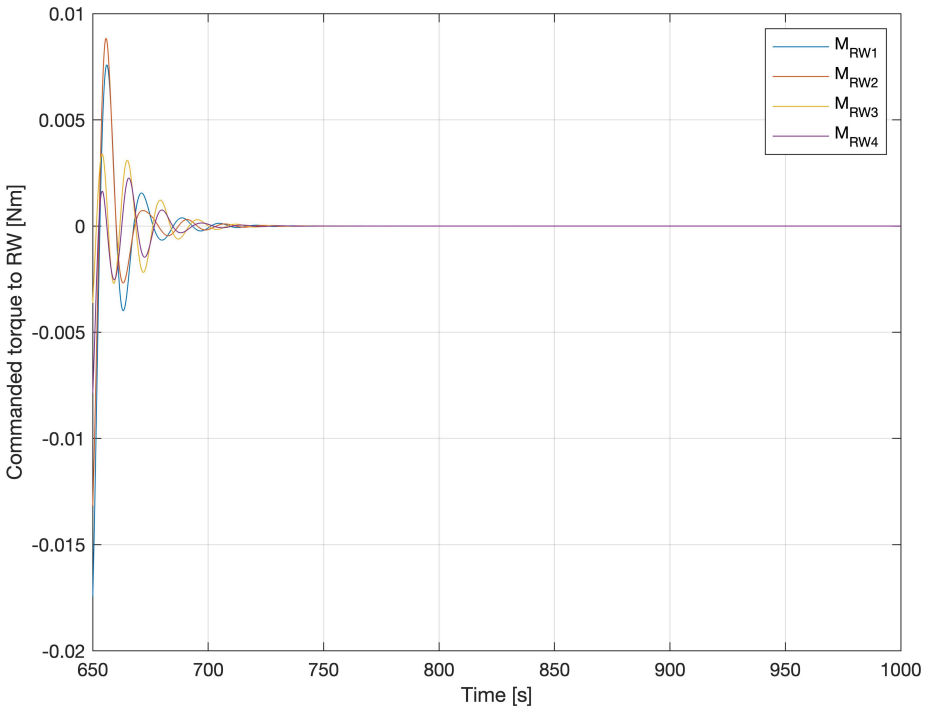

Figure 4.11: Torque commanded to the reaction wheels in time - Manoeuvre 2

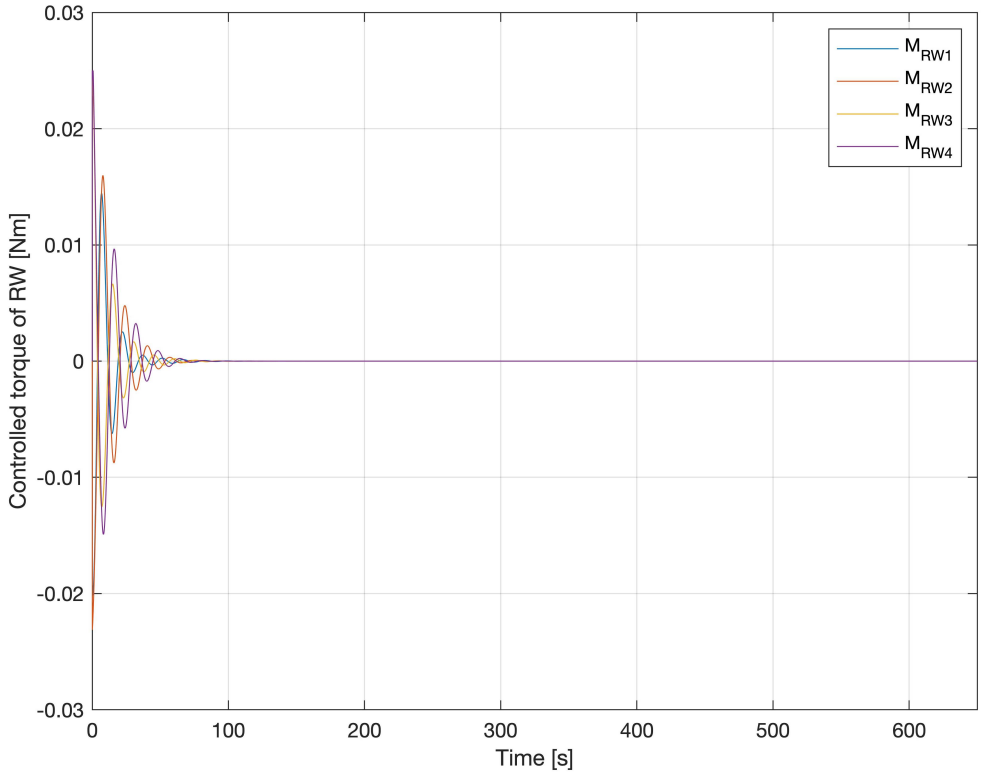

Figure 4.12: Controlled torque of the reaction wheels in time - Manoeuvre 1

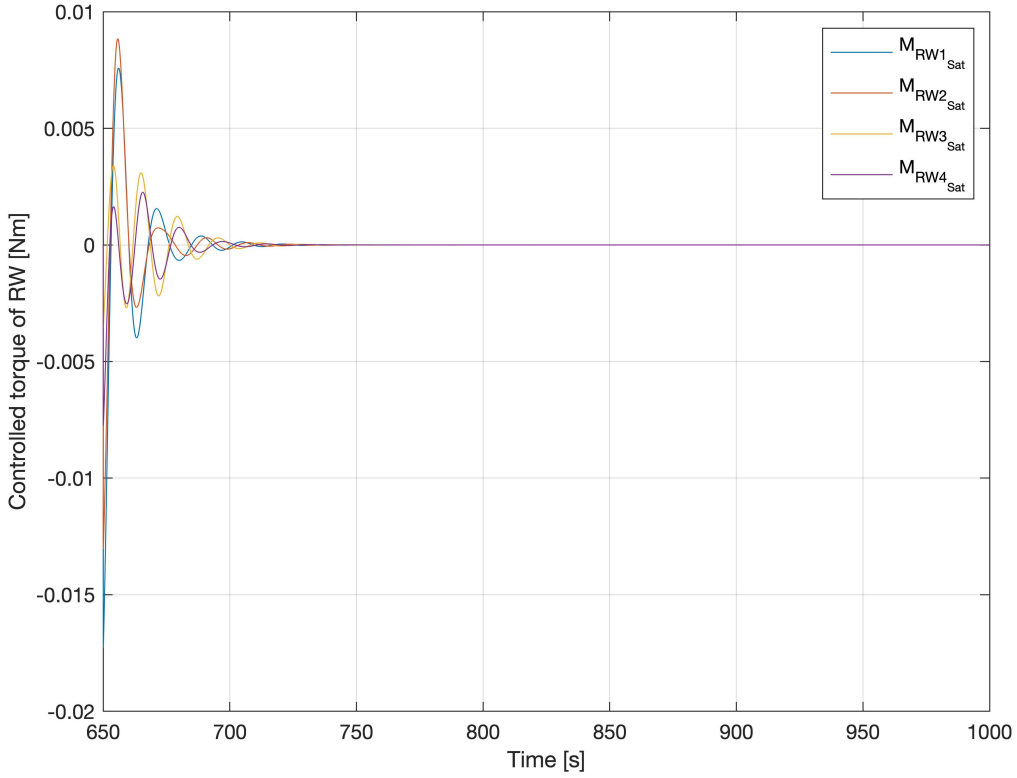

Figure 4.13: Controlled torque of the reaction wheels in time - Manoeuvre 2

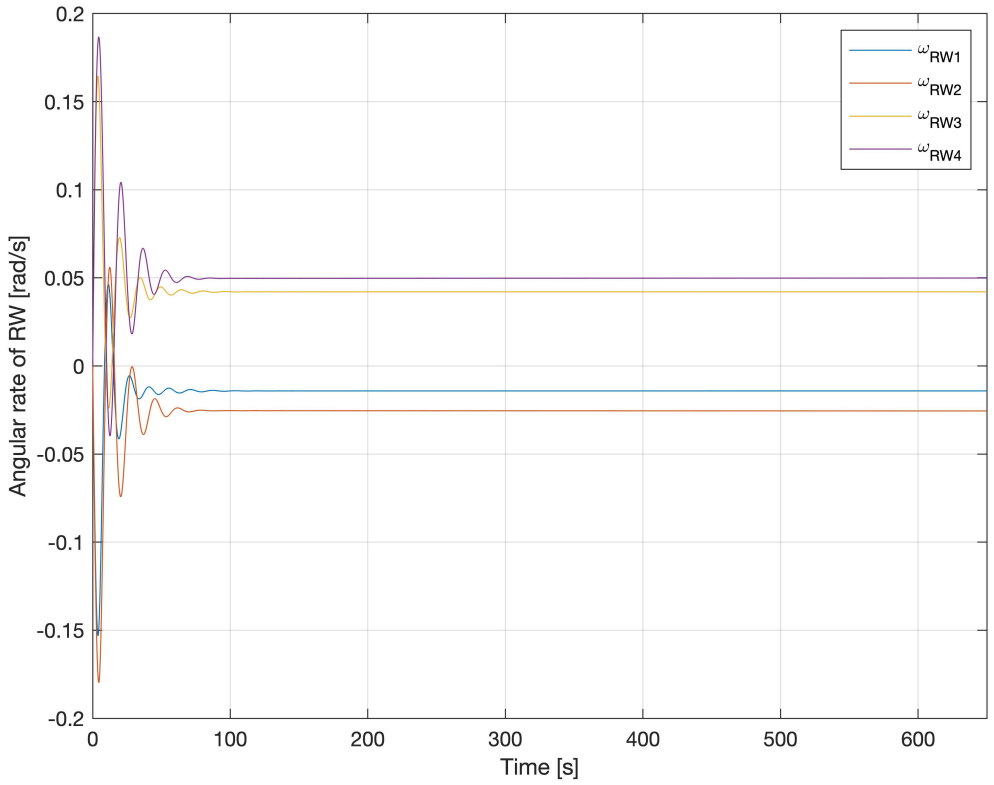

Figure 4.14: Angular rate of the reaction wheels in time - Manoeuvre 1

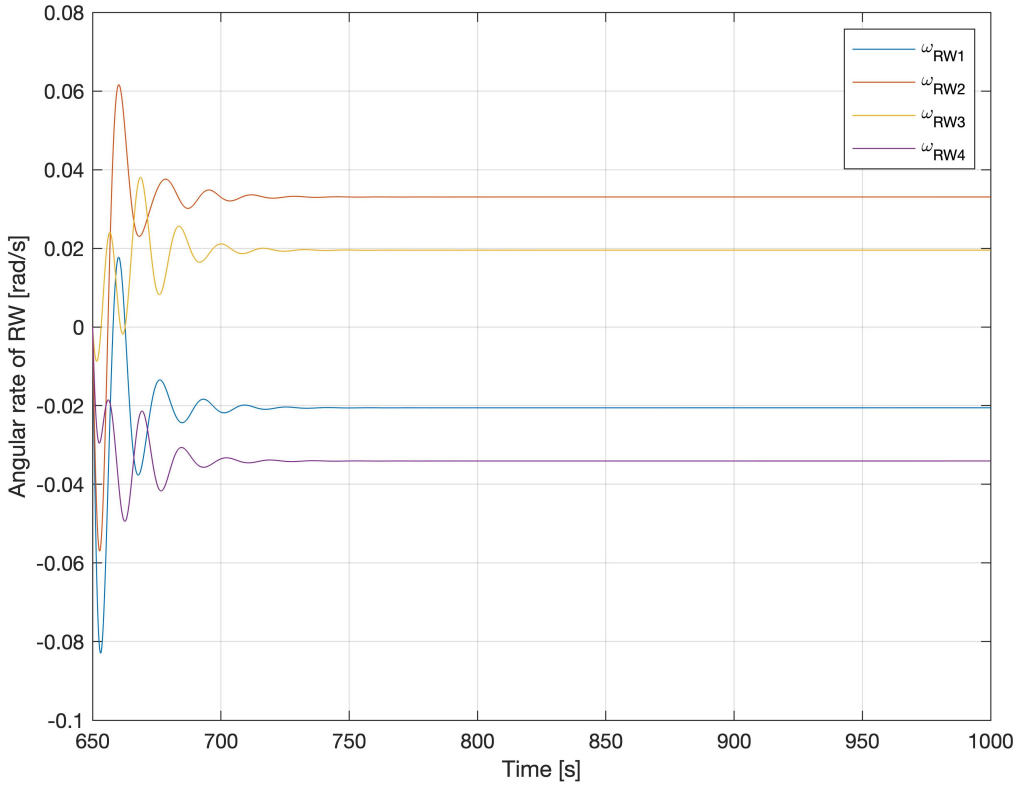

Figure 4.15: Angular rate of the reaction wheels in time - Manoeuvre 2

4.3. Debris closing and observation results

The numerical results of the closing phase of this mission are summarized in the following tables. The final positions that the chaser has reached at the end of each radial boost using the proposed guidance algorithms are shown in the Table 4.3 and the relative velocity with respect to the target at those points in Table 4.4. The total time that the chaser has needed to arrive to the final position with each algorithm is: $T_{id} = 17004.42$ s, $T_{PNG_1} = 8035.24$ s, $T_{PNG_2} = 8533.75\ s$ and $T_{CTVG} = 9000$ s.

	Ideal case		**PNG$_1$**		**PNG$_2$**		**CTVG**	
	X_f	Z_f	X_f	Z_f	X_f	Z_f	X_f	Z_f
1st	-500	0	-713.993	-0.007	-573.092	-0.005	-500.135	-0.092
2nd	-200	0	-243.436	$-7.396{\cdot}10^{-4}$	-210.098	$-9.809{\cdot}10^{-5}$	-200.024	-0.011
3rd	-50	0	-65.820	$-4.595{\cdot}10^{-4}$	-53.686	$-7.788{\cdot}10^{-5}$	-50.017	-0.001

Table 4.3: Closing phase - Final position at the end of each radial boost. All values are given in ISU

Taking the ideal case as reference, if we look the results obtained with the Proportional Navigation law with configuration 1, the errors in position are very large comparing with the other algorithms used, especially on the first and second boosts in which the deviation in position in the x-axis up to about 214 m and 43 m, but it is reduced to only about 16 m at the end of the whole manoeuvre.

On the other side, using the second configuration in which the control system has a feedback of the current state of the chaser, as it was expected, the error position has diminished in all three manoeuvres. At the end of the first manoeuvre is about 73 m, however, it has been properly corrected during the second and third boosts, in which the position deviation are about 10 m and only of 4 m at the end of the whole closing phase.

Finally, the results obtained using the CTVG guidance are really good. As can be observed, during the whole manoeuvres the errors in the x-axis is only about 13 cm at the end of the first boost and it is reduced to only 2 cm ad the end of the third radial boost. Using this control law, the error in the z-axis are a little larger than in the other two cases, anyway it has been reduced to only 1 mm.

	Ideal case		**PNG$_1$**		**PNG$_2$**		**CTVG**	
	V_{x_f}	V_{z_f}	V_{x_f}	V_{z_f}	V_{x_f}	V_{z_f}	V_{x_f}	V_{z_f}
1st	0	0	-0.03	-0.7493	-0.026	-0.648	$4.962{\cdot}10^{-4}$	$-9.385{\cdot}10^{-5}$
2nd	0	0	-0.006	-0.153	-0.004	-0.096	$5.950{\cdot}10^{-5}$	$-1.120{\cdot}10^{-5}$
3rd	0	0	-0.003	-0.057	-0.002	-0.041	$2.974{\cdot}10^{-5}$	$-5.596{\cdot}10^{-6}$

Table 4.4: Closing phase - Final relative velocity at the end of each radial boost. All values are given in ISU

Regarding the relative velocity, it can be observed that when using the second configuration of the PNG also the velocity errors are reduced with respect to the first one. However, in both cases the spacecraft still having a certain velocity that will have to be compensated.

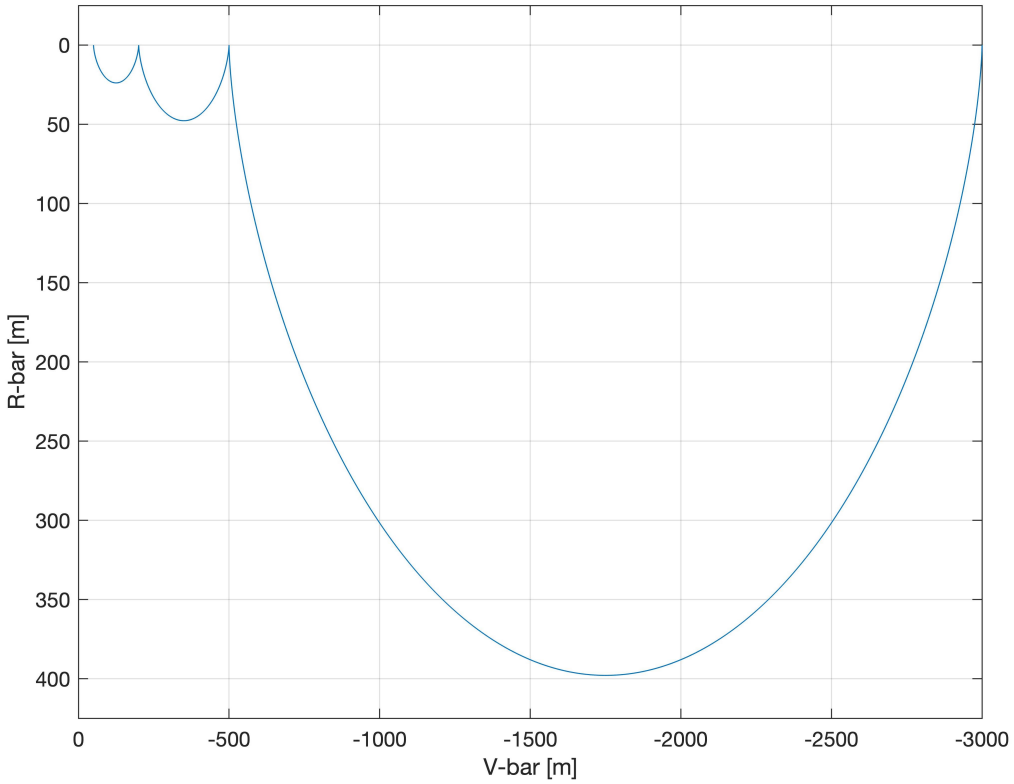

Figure 4.16: Closing phase trajectory - Ideal case

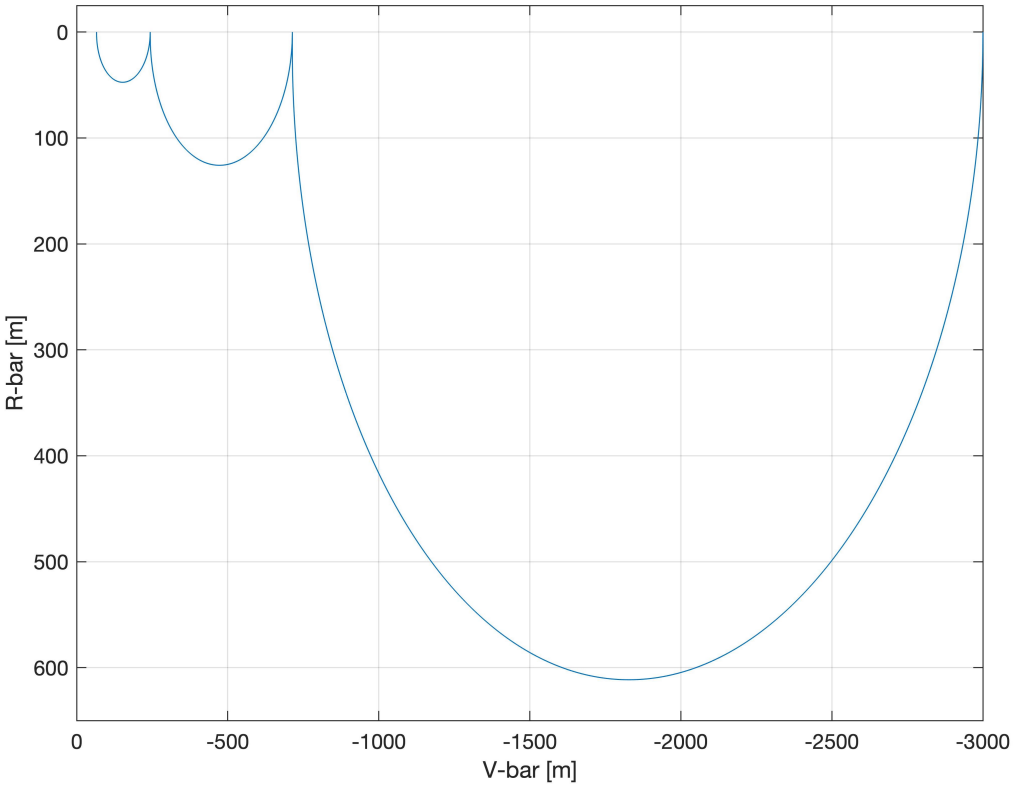

Figure 4.17: Closing phase trajectory - PNG Conf. 1

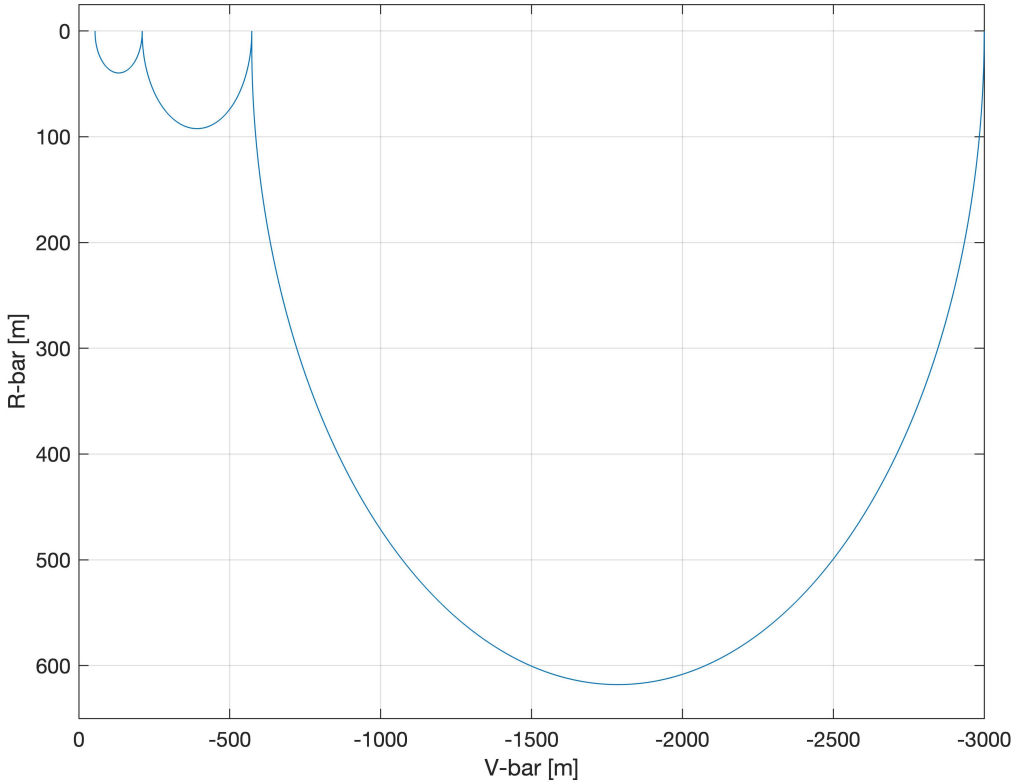

Figure 4.18: Closing phase trajectory - PNG Conf. 2

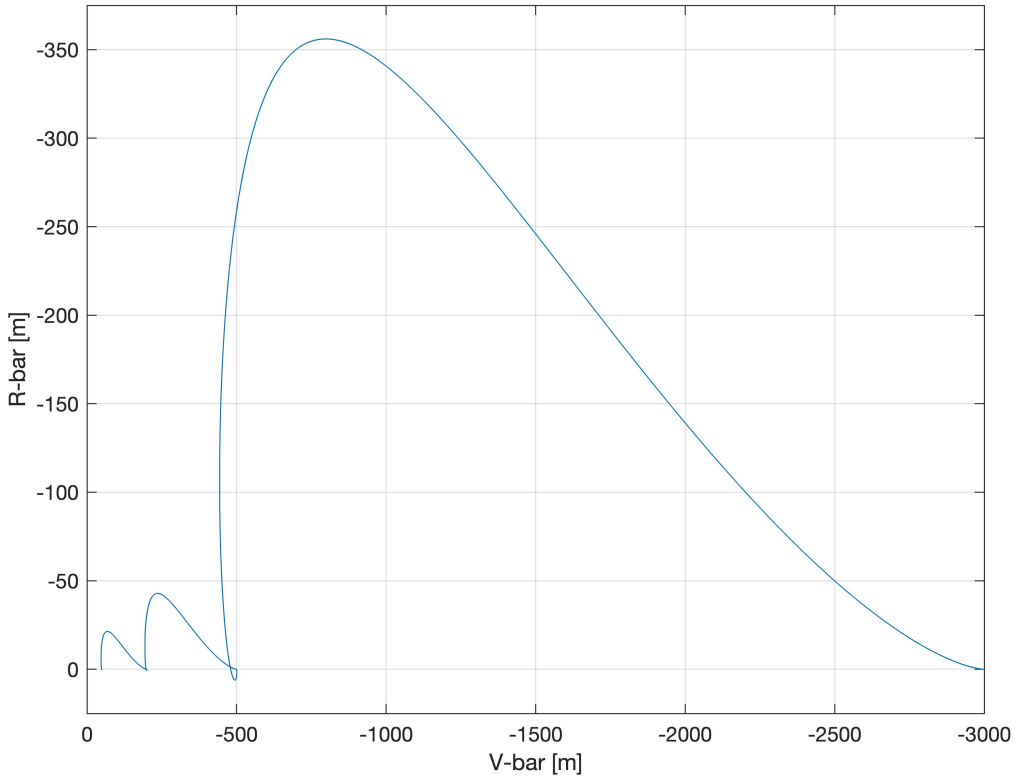

Figure 4.19: Closing phase trajectory - CTVG

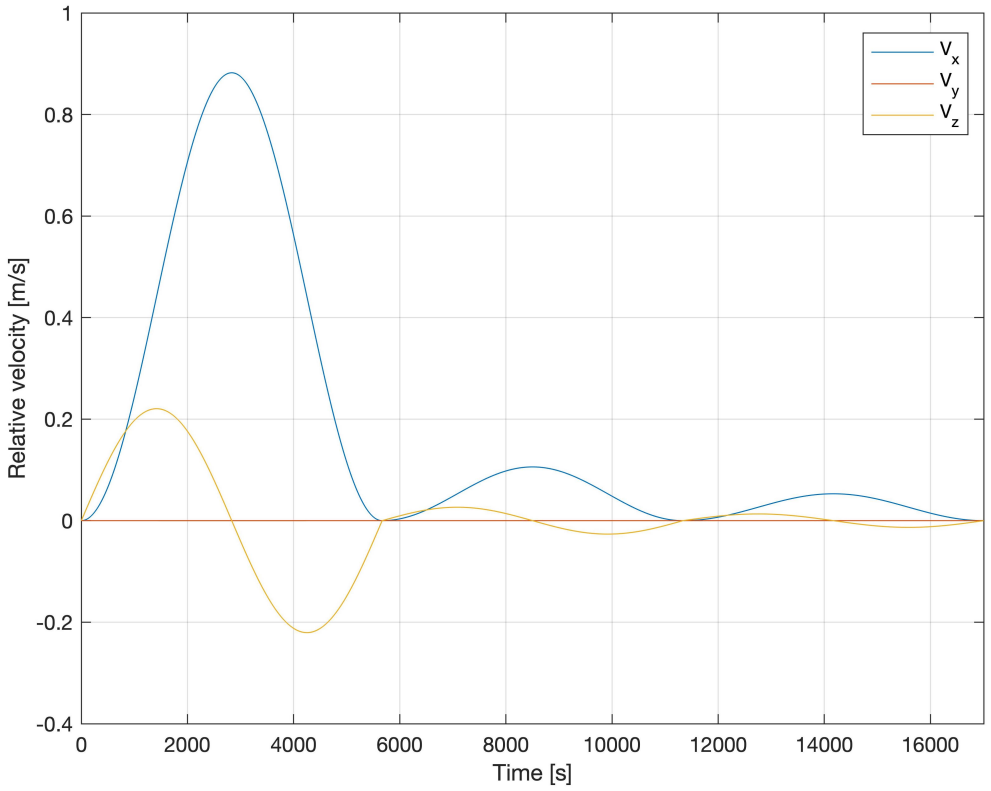

Figure 4.20: Relative velocity in time - Ideal case

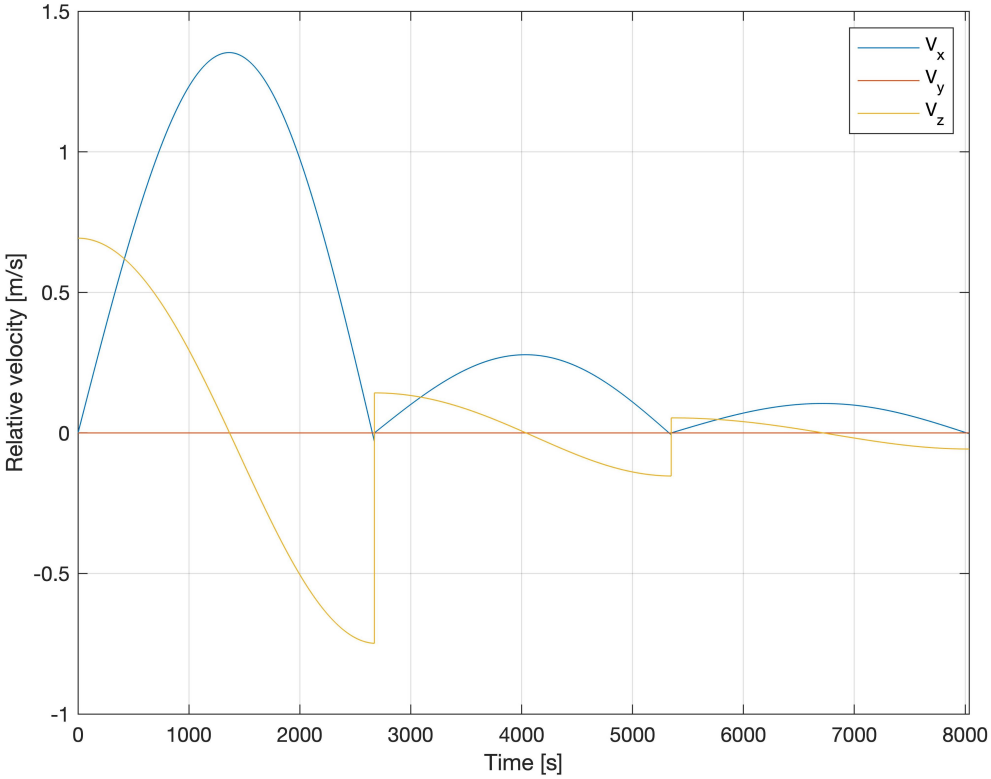

Figure 4.21: Relative velocity in time - PNG Conf. 1

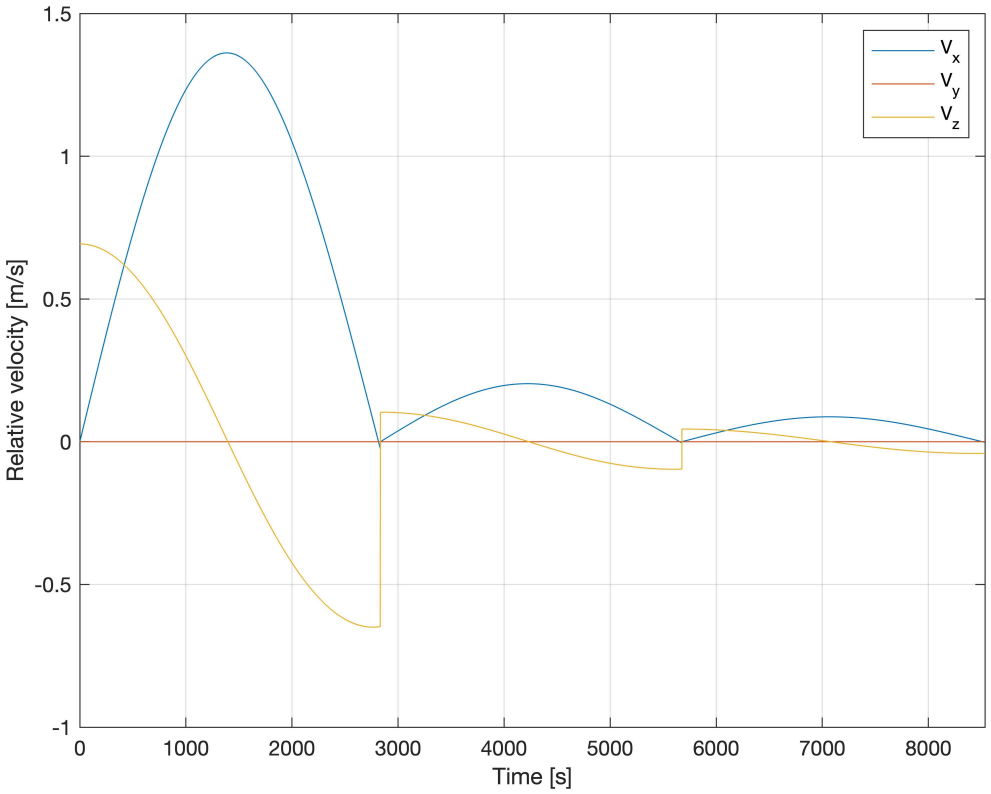

Figure 4.22: Relative velocity in time - PNG Conf. 2

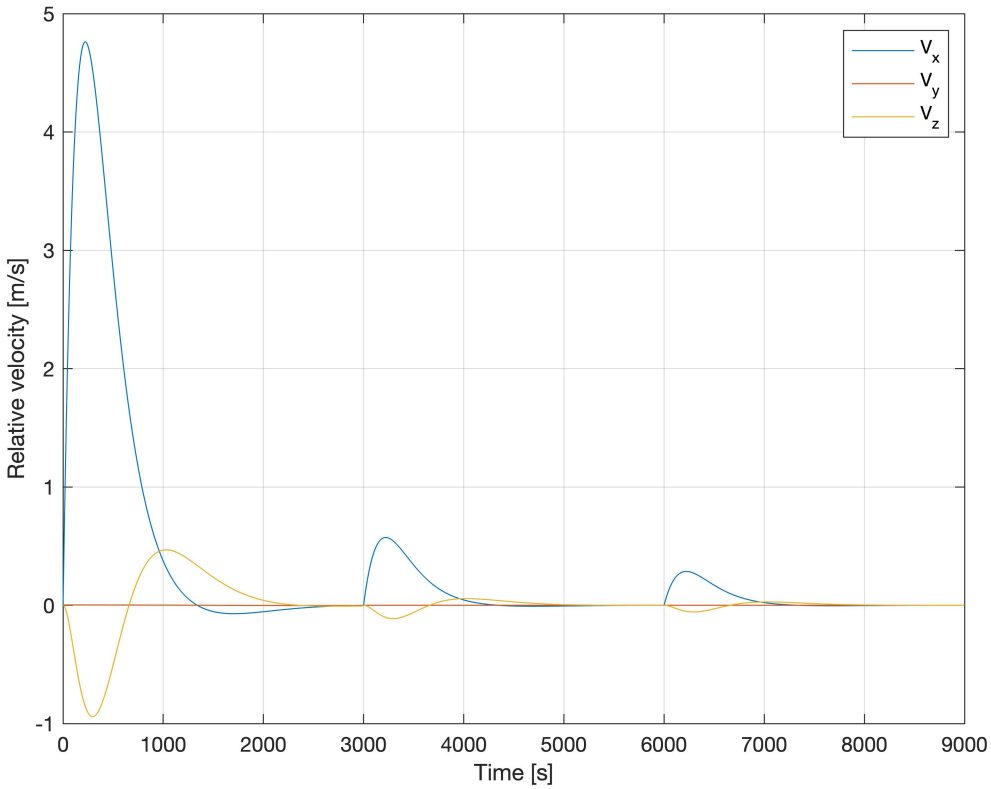

Figure 4.23: Relative velocity in time - CTVG

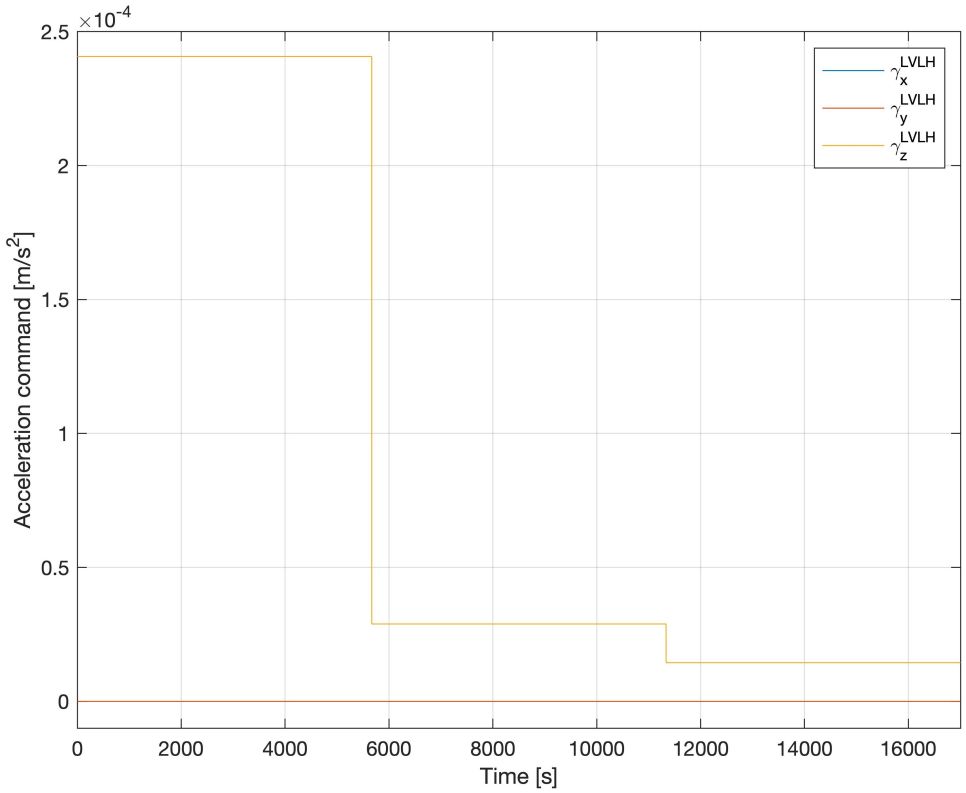

Figure 4.24: Acceleration command in time - Ideal case

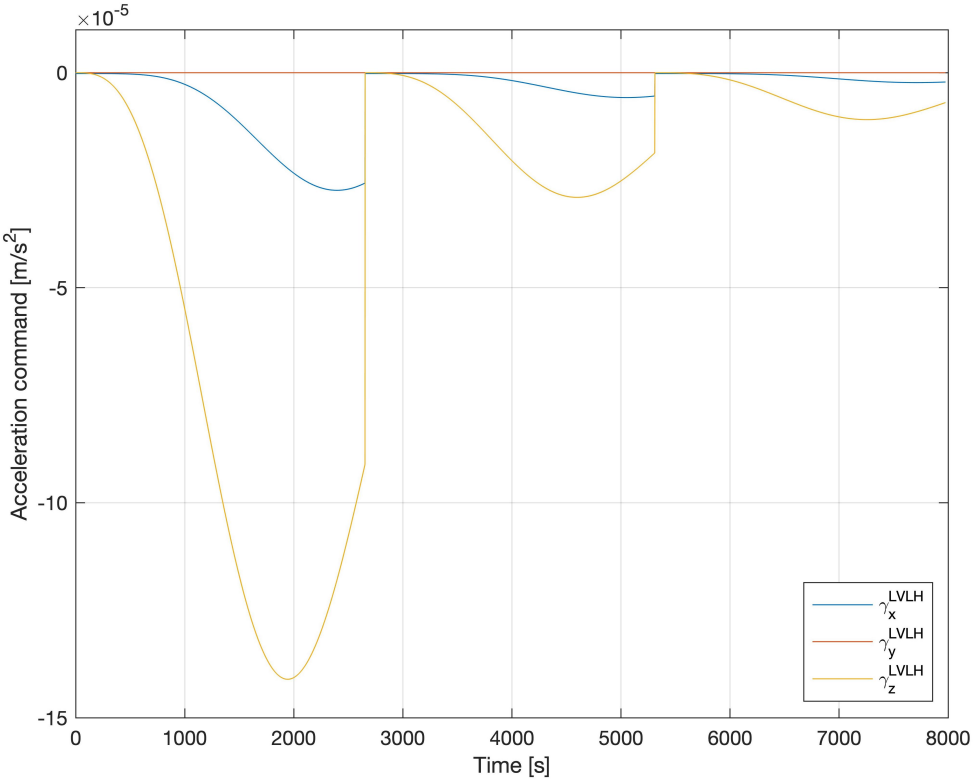

Figure 4.25: Acceleration command in time - PNG Conf. 1

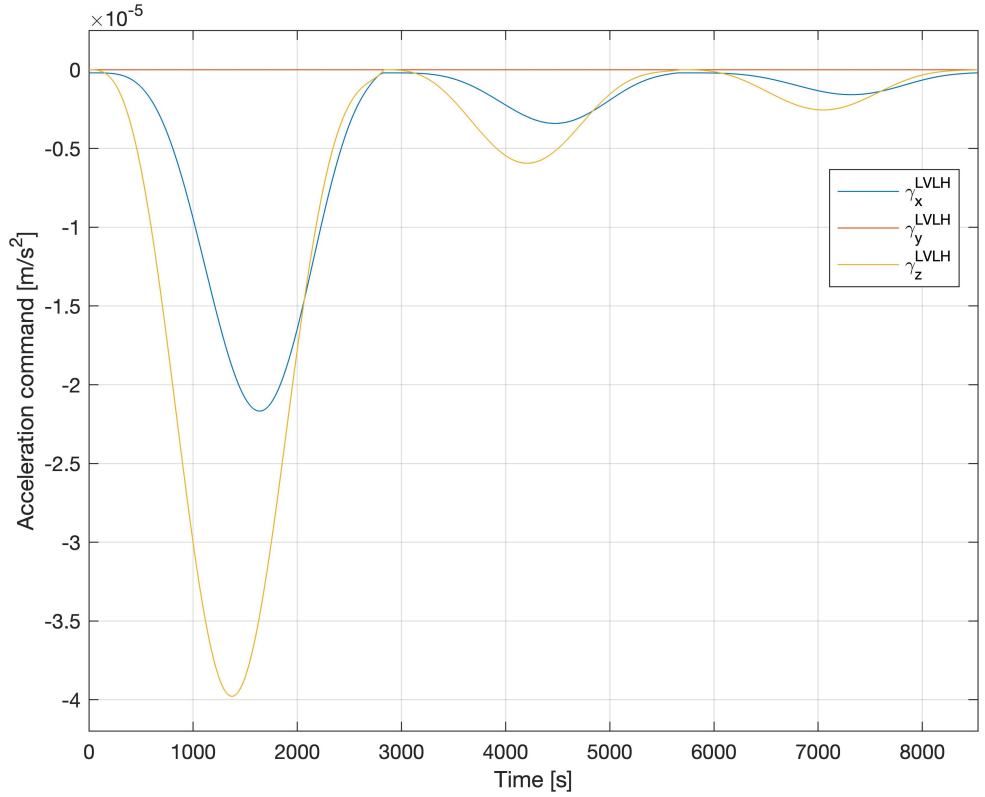

Figure 4.26: Acceleration command in time - PNG Conf. 2

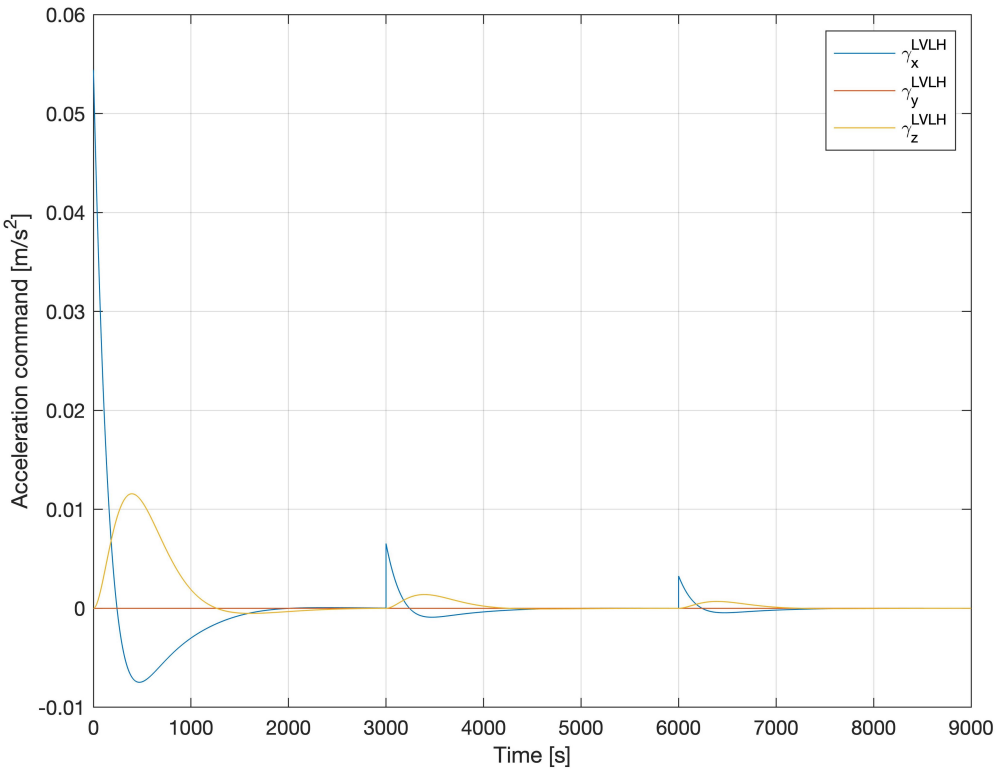

Figure 4.27: Acceleration command in time - CTVG

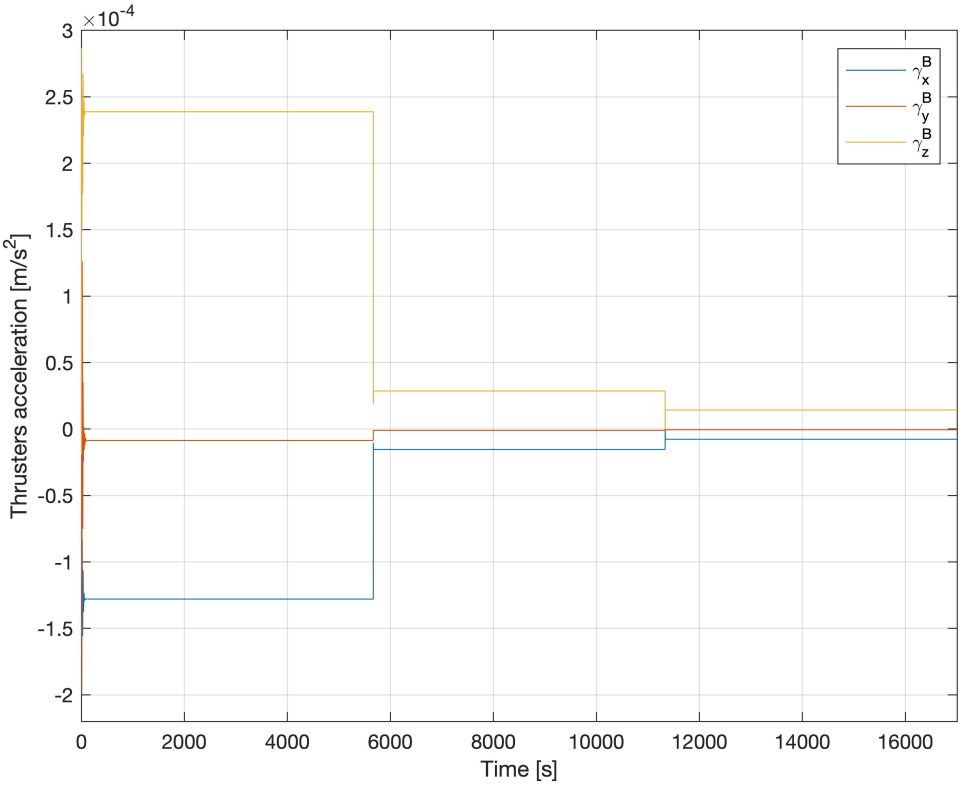

Figure 4.28: Thrusters saturated acceleration in time - Ideal case

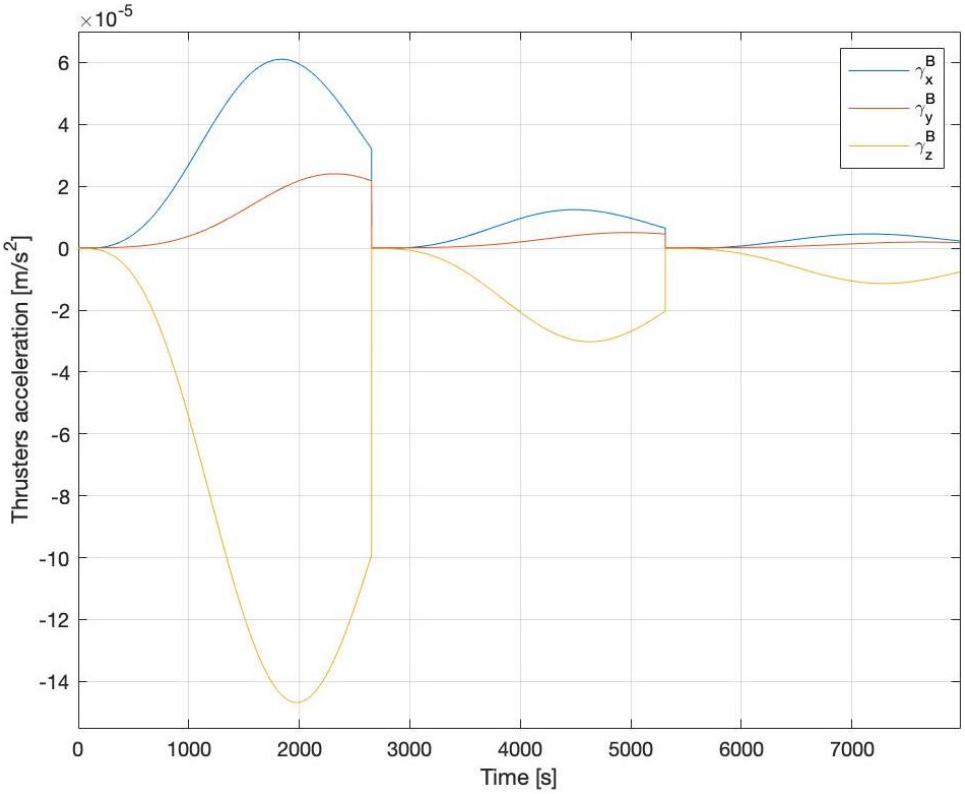

Figure 4.29: Thrusters saturated acceleration in time - PNG Conf. 1

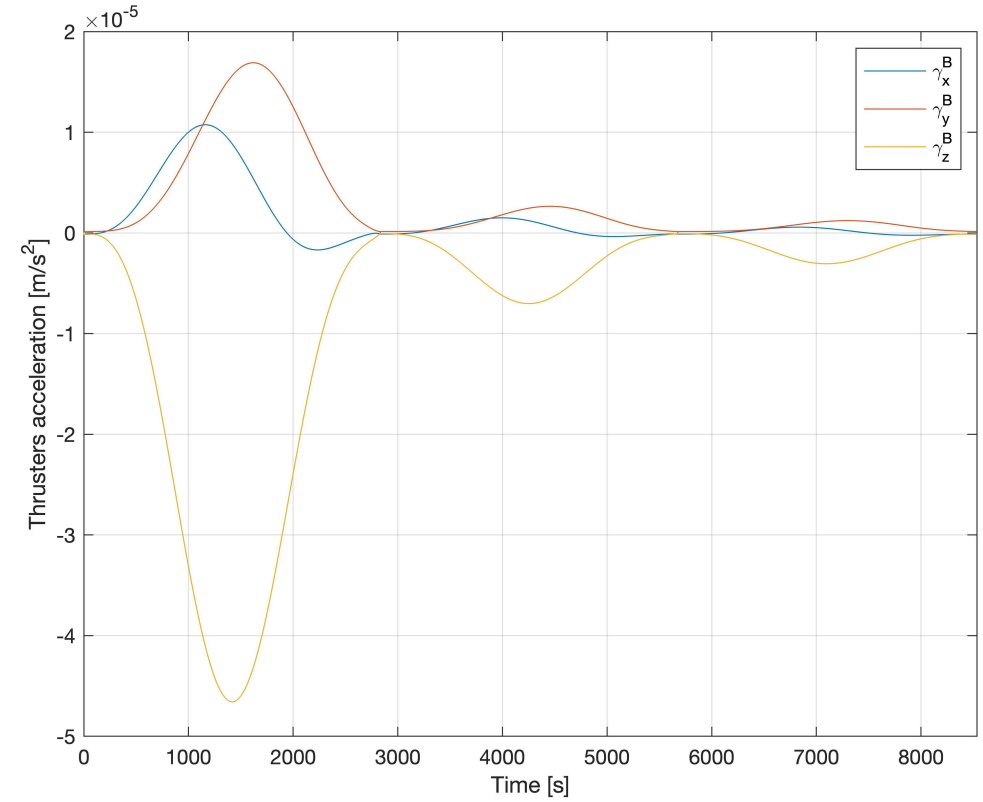

Figure 4.30: Thrusters saturated acceleration in time - PNG Conf. 2

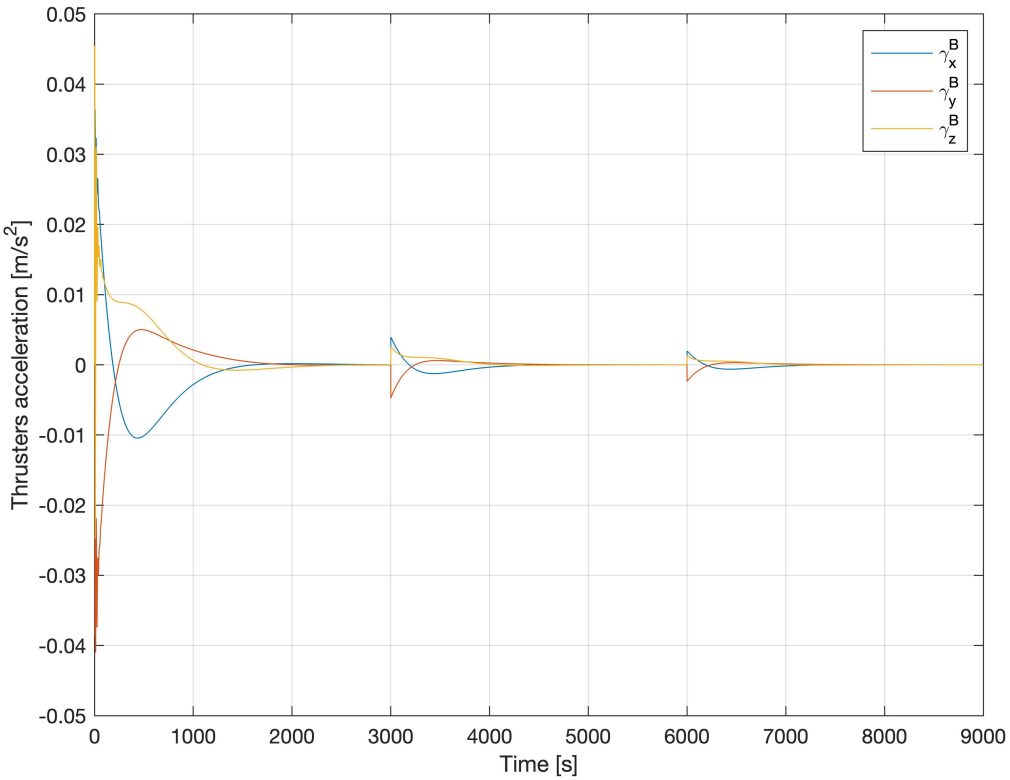

Figure 4.31: Thrusters saturated acceleration in time - CTVG

From the results in this mission and looking at Figure 4.32, in which all the trajectories are compared, all three algorithms that have been implemented have worked, although some with better effectiveness than the others.

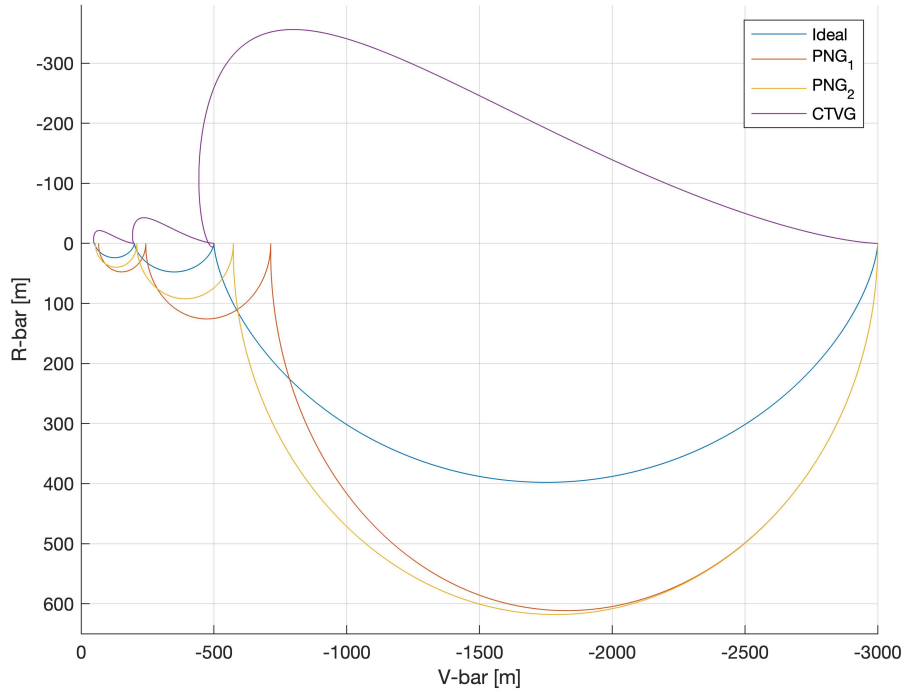

Figure 4.32: Closing trajectories comparison

In the following table are shown the values of the optimization parameter from Eq. 3.7, in which the CTVG algorithm is based, for all the algorithms that have been implemented:

	Ideal case	**PNG$_1$**	**PNG$_2$**	**CTVG**
Performance index J	0.03448	0.00252	0.00018	25.30122

Table 4.5: Performance index of the different guidance algorithms

As can be observed, the algorithms that were trying to follow the reference trajectory of the ideal case have obtained really low values in the performance index compared with the CTVG law. However, from the results obtained in the simulations it is note that the algorithm with a higher value of the performance index also has had a better performance, instead, the PNG algorithms have had larger errors in both position and velocity that will have to be properly corrected.

Regarding the observation phase of this mission, the objective was to reach the desired attitude during the first radial boost and keep it constant until the end of the closing operation in order to start the final approach phase with the satellite pointing towards the objective.

Since, ideally, the propulsion system does not introduce any disturbance to the spacecraft thanks to the proposed configuration, as it was expected the attitude results are exactly the same using all different algorithms. Then, only the results in the ideal case have been collected because is the one that takes longer to arrive to the final position.

	Observation phase - 1st radial boost			
	q_0	q_1	q_2	q_3
$\mathbf{q}_{des}$	0.8365	-0.1294	0.2241	0.4830
$\mathbf{q}_f$	0.836506	-0.129403	0.224100	0.483004
$\mathbf{q}_{err}$	1.000007	$-2.733458 \cdot 10^{-6}$	$-1.334242 \cdot 10^{-10}$	$-2.757239 \cdot 10^{-7}$
	ϕ	θ	ψ	
$[\phi, \theta, \psi]_{err}$	$-5.466878 \cdot 10^{-6}$	$-2.683577 \cdot 10^{-10}$	$-5.514440 \cdot 10^{-7}$	
	ω_x	ω_y	ω_z	
ω_f	$-2.451403 \cdot 10^{-15}$	$-2.382399 \cdot 10^{-15}$	$3.293510 \cdot 10^{-15}$	

Table 4.6: Observation phase - Final attitude and angular rate at the end of the first radial boost. All values are given in ISU.

	Observation phase - 2nd radial boost			
	q_0	q_1	q_2	q_3
$\mathbf{q}_{des}$	0.8365	-0.1294	0.2241	0.4830
$\mathbf{q}_f$	0.836506	-0.129403	0.224100	0.483004
$\mathbf{q}_{err}$	1.000007	$-2.733458 \cdot 10^{-6}$	$-1.334276 \cdot 10^{-10}$	$-2.757239 \cdot 10^{-7}$
	ϕ	θ	ψ	
$[\phi, \theta, \psi]_{err}$	$-5.466878 \cdot 10^{-6}$	$-2.683642 \cdot 10^{-10}$	$-5.514440 \cdot 10^{-7}$	
	ω_x	ω_y	ω_z	
ω_f	$9.464616 \cdot 10^{-16}$	$4.249804 \cdot 10^{-16}$	$-4.455782 \cdot 10^{-15}$	

Table 4.7: Observation phase - Final attitude and angular rate at the end of the second radial boost. All values are given in ISU.

	Observation phase - 3rd radial boost			
	q_0	q_1	q_2	q_3
$\mathbf{q}_{des}$	0.8365	-0.1294	0.2241	0.4830
$\mathbf{q}_f$	0.836506	-0.129403	0.224100	0.483004
$\mathbf{q}_{err}$	1.000007	$-2.733458 \cdot 10^{-6}$	$-1.334276 \cdot 10^{-10}$	$-2.757239 \cdot 10^{-7}$
	ϕ	θ	ψ	
$[\phi, \theta, \psi]_{err}$	$-5.466878 \cdot 10^{-6}$	$-2.683647 \cdot 10^{-10}$	$-5.514440 \cdot 10^{-7}$	
	ω_x	ω_y	ω_z	
ω_f	$9.461735 \cdot 10^{-16}$	$3.972544 \cdot 10^{-16}$	$-4.456669 \cdot 10^{-15}$	

Table 4.8: Observation phase - Final attitude and angular rate at the end of the third radial boost. All values are given in ISU.

As can be observed in Figure 4.33 and looking at the results of Table 4.6, the satellite has reached the desired attitude in about 150 s after the beginning of the simulation with a precision of $\pm 0.0003^{o}$ with practically null angular velocity. On the other side, from Figure 4.34 and Table 4.7 and 4.8 it can be seen that the control system has been able to maintain it with that orientation during the whole manoeuvre.

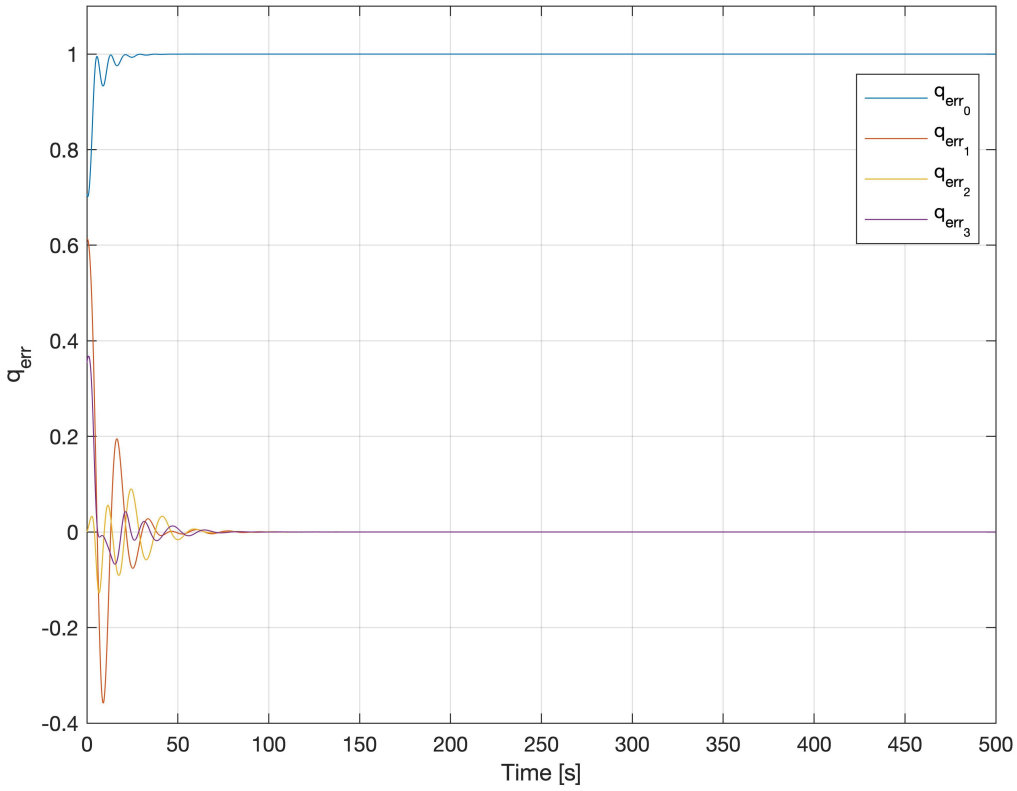

Figure 4.33: Quaternions error in time during the firts 500 s of the simulation

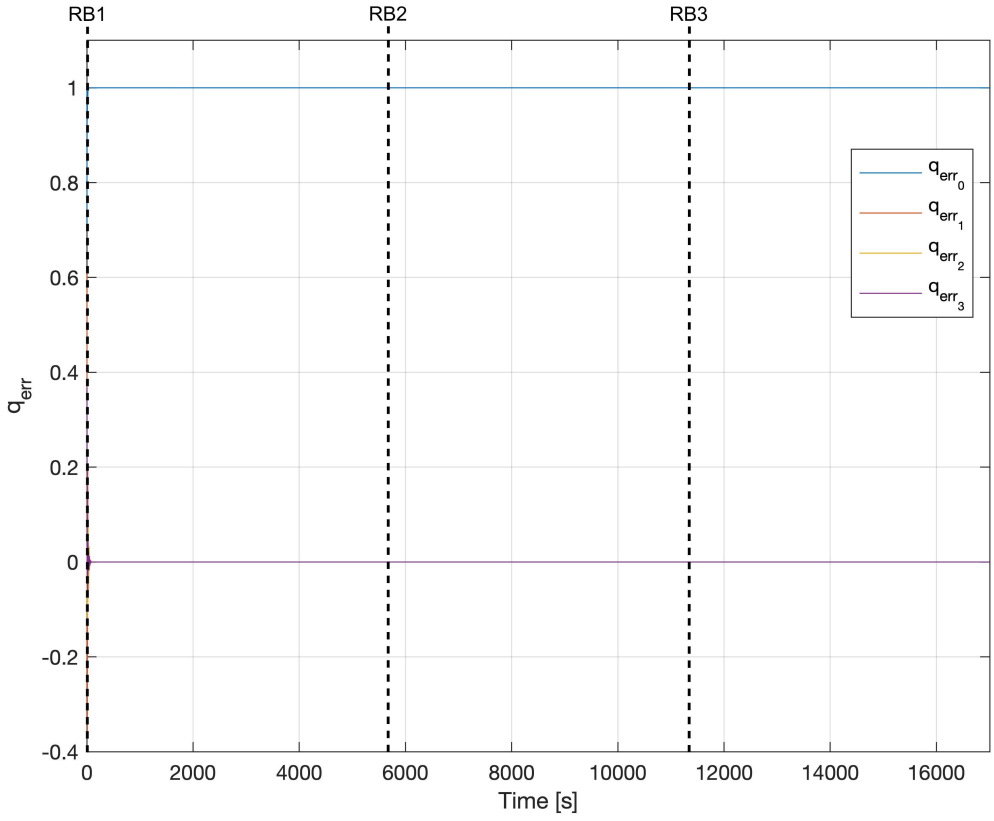

Figure 4.34: Quaternions error in time during the whole closing phase - Ideal case

CONCLUSIONS

The main goal of this research project was to design a functional control system able to control properly the orbital and attitude dynamics of a small satellite for precise pointing missions. Thus, in order to evaluate the functioning of the system, a rendezvous maneuver between a Chaser and Target is considered. Two main simulation scenarios are proposed:

- **Crab Nebula observation**, in which the spacecraft must perform two pointing manoeuvres, the first one towards the Crab Nebula in order to collect some data.
- **Debris closing and observation**, in which the chaser must perform the closing phase of a rendezvous process to get closer of a space debris satellite and reach the proper attitude to capture it.

For the orbital dynamics, a relative motion is analyzed by Hill's equations, in which a local orbital frame is defined. Moreover, circular orbits and relative motion between two spacecraft are assumed. Then, to compute the input acceleration commands needed to reach the desired position, two different guidance algorithms have been tested: (1) a **Proportional Navigation** law, evaluated in two different configurations; (2) and an optimal guidance algorithm named **Constrained Terminal Velocity Guidance**.

On the other side, the attitude dynamics of the spacecraft are analyzed by quaternions and Euler's equations, in a body frame centred at the CoM of the chaser. The attitude control is done by 4 reaction wheels disposed in a square pyramid configuration and the control torques to be applied are computed by means of a **PD controller**, tuned manually.

After carrying out the simulations of the two proposed scenarios, regarding the **orbital control** it can observed from the obtained results that both guidance algorithms that have been implemented, PN (Conf. 1 and 2) and CTVG, have work correctly. In all three cases, the position error at the end of each boost has been reduced, obtaining errors at the end of the whole manoeuvre of about 16 m and 4 m with an error of some decimetres per second in the final velocity for PN Conf. 1 and PN Conf. 2, respectively, and 0.02 m with practically no velocity error for CTVG.

Regarding the **attitude control**, from both scenarios can be observed that the pointing precision achieved by the system is about $\pm 0.0003^{o}$, and from the Debris closing and observation mission, it can be seen that the system is also able to keep the satellite pointing towards the same attitude for long periods of time, that may be interesting in observation missions but also for capture or docking missions. In all simulations the system starts with some oscillations that are practically attenuated at all after about 100 s. Then, the desired position is always reached after about 170-200 s.

Thus, it can be concluded that the control system for both translational and rotational dynamics of the satellite that has been designed works in a correct way and, then, it can be considered that the initial objective has been achieved.

As future work, it could be also interesting to consider the design of a control function able to perform the final approach phase of the rendezvous process. In this way the whole close-range phase could be evaluated.

BIBLIOGRAPHY

[1] "Cronología de la astronomía".
https://www.astronomia-iniciacion.com/cronologia-astronomia.html

[2] "Los primeros astrónomos".
https://sites.google.com/site/nfjhgfrjhdlkjhlk/

[3] "Principales astrónomos".
https://sites.google.com/site/elmundodelaastronomia/
-que-es-la-astronomia/principales-astronomos

[4] "Apollo 11 Command and Service Module (CSM)". NASA Space Science Data Coordinated Archive. Retrieved November 20, 2019.
https://nssdc.gsfc.nasa.gov/nmc/spacecraft/display.action?id=
1969-059A

[5] "Lanzamiento del Sputnik I".
https://canalhistoria.es/hoy-en-la-historia/
lanzamiento-del-sputnik-i/

[6] "How many satellites are orbiting earth in 2018". Pixalytics. 22 August 2018. Retrieved 27 September 2018.
https://www.pixalytics.com/sats-orbiting-the-earth-2018/

[7] "ESA commissions world's first space debris removal".
https://www.esa.int/Safety_Security/Clean_Space/ESA_commissions_
world_s_first_space_debris_removal

[8] "ELSA-d (End-of-Life Service by Astroscale)-d (demonstration)".
https://directory.eoportal.org/web/eoportal/satellite-missions/
content/-/article/elsa-d

[9] Popescu, G., "Pixel Geolocation Algorithm for Satellite Scanner Data", University of Agronomic Sciences Veterinary Medicine of Bucharest.

[10] Bloise, N.,Capello, E., Dentis, M., Punta, E., "Obstacle Avoidance with Potential Field Applied to a Rendezvous Maneuver", *Applied Sciences*, 7, 1042, 2017.

[11] "The Different Frames and the Keplerian Elements".
https://adcsforbeginners.wordpress.com/tag/inertial-frame-of-reference/

[12] Fehse, W., *Automated Rendezvous and Docking of Spacecraft*, Rycroft, M.J., Shyy, W., Cambridge Univ. Press, New York, Chaps. 2, 3 and 6, 2003.

[13] Arias, S., "Notes on Euler Angles", Universitat Politècnica de Catalunya, Spain.

[14] Olguín Díaz, E., *3D Motion of Rigid Bodies: A Foundation for Robot Dynamics Analysis*, Vol. 191, J. Kacprzyk, Warsaw, Poland, pp. 160-164.

[15] Abaunza González, H., "Robust Tracking of Dynamic Targets with Aerial Vehicles Using Quaternion-based Techniques", PhD Thesis, Université de Technologie de Compiègne, 2019.

[16] Xing, G.Q., Paverz, S.A., “Alternate forms of relative attitude kinematics and dynamics equations”, Space Products and Applications Inc., Fairfax, VA, 2001.

[17] Särkkä, S., “Notes on Quaternions”, Aalto University, Aalto, Finland, 2007.

[18] De Ruiter, A.H.J., Damaren, C.J., Forbes, J.R., *Spacecraft Dynamics and Control*, United Kingdom, 2013.

[19] Capello, E., “Notes on Position and Attitude Dynamics”, Politecnico di Torino, Italy.

[20] Capello, E., “Notes on Actuators for position and attitude control”, Politecnico di Torino, Italy.

[21] Vazquez, R., Gavilan, F., Camacho, E.F., “Trajectory Planning for Spacecraft Rendezvous in Elliptical Orbits with On/Off Thrusters”, Universidad de Sevilla, Sevilla, Spain.

[22] N. Carnevaletti, “Design of Robust Control Techniques for a Small Satellite with Flexible Appendages”, Master Thesis, Politecnico di Torino, 2020.

[23] Capello, E., Dentis, M., “Precise Attitude Control Techniques: Performance Analysis from Classical to Variable Structure Control”, Politecnico di Torino, Italy, 2019.

[24] Federal Aviation Administration, “Advanced Aerospace Medicine”, Section III, 2018.

[25] Yazhong, L., Jin, Z., Guojin, T., “Survey of orbital dynamics and control of space rendezvous”, *Chinese Journal of Aeronautics*, Vol. 27, pp. 1-11, 2014.

[26] Squires, D., “1HOPSat formal orbital debris assessment report (ODAR) and end of mission plan (EOMP)”, Hera Systems, Tech. Rep. 3, 2018.

[27] Capello, E., Punta, E., Dabbene, F., Guglieri, G., Tempo, R., “Sliding-Mode Control Strategies for Rendezvous and Docking Maneuvers”, *Journal of Guidance, Control and Dynamics*, Vol. 40, No. 6, pp. 1481-1488, 2017.

[28] Cipro, F., Park, H., Capello, E., “CubeSat Attitude Control Systems based on LPV and Twisting Sliding Mode Methods”, *59th IEEE Conference on Decision and Control (CDC)*, 2020.

[29] N. Carnevaletti, “Robust attitude control and failure analysis for small satellites”, Master Thesis, Politecnico di Torino, 2019.

[30] Zarchan, P., *Tactical and Strategic Missile Guidance*, 5th Ed., Progress in Astronautics and Aeronautics, AIAA, Washington, DC, 2007.

[31] Cicolani, L.S., “Trajectory Control in Rendezvous Problems Using Proportional Navigation”, National Aeronautics and Space Administration, Washington, 1961.

[32] Capello, E., Dabbene, F., Guglieri, G., Punta, E., “Flyable Guidance and Control Algorithms for Orbital Rendezvous Maneuver”, *Journal of Control, Measurement and System Integration*, Vol. 11, No. 1, pp. 14-24, 2018.

[33] Hawkins, M., Guo, Y., Wie, B., “Spacecraft Guidance Algorithms for Asteroid Intercept and Rendezvous Missions”, *International Journal of Aeronautical and Space Sciences*, Vol. 13, No. 2, pp. 154-169, 2012.

[34] Guo, Y., Hawkins, M., Wie, B., “Optimal Feedback Guidance Algorithms for Planetary Landing and Asteroid Intercept”, *AAS/AIAA Astrodynamics Specialist Conference*, AAS Paper No. 11-588, 2011.

[35] Hawkins, M., “New near-optimal feedback guidance algorithms for space missions”, *Graduate Theses and Dissertations*, 13103, 2013.

[36] Hawkins, M., Guo, Y., Wie, B., “Guidance algorithms for asteroid intercept missions with precision targeting requirements”, *AAS/AIAA Astrodynamics Specialist Conference*, AAS Paper No. 11-531, 2011.

[37] Hegrenas, O., “Attitude control by means of explicit Model Predictive Control, via Multi-parametric Quadratic Programming”, 2004.

APPENDICES

APPENDIX A. SIMULINK MODELS

A.1. Orbit control models

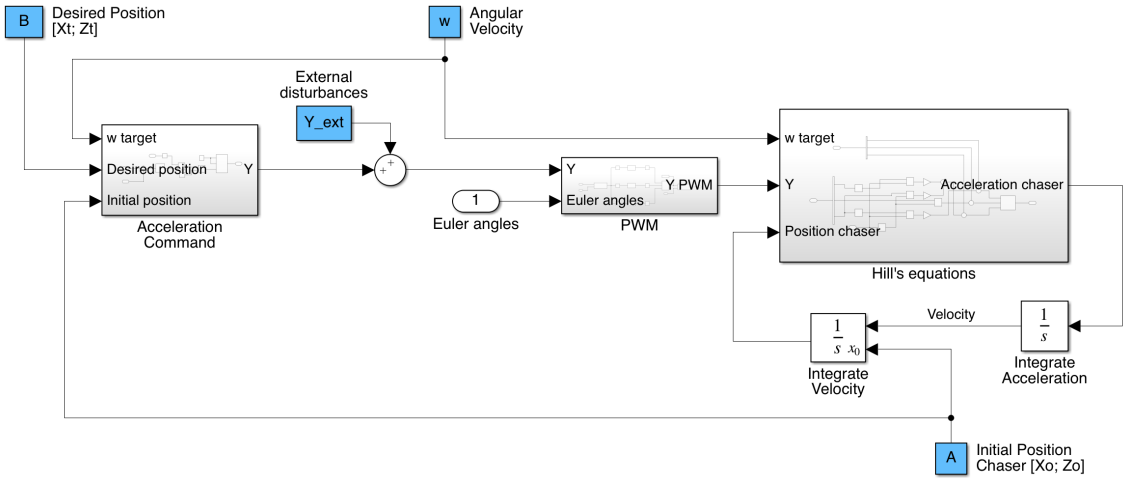

Figure A.1: Orbit control model

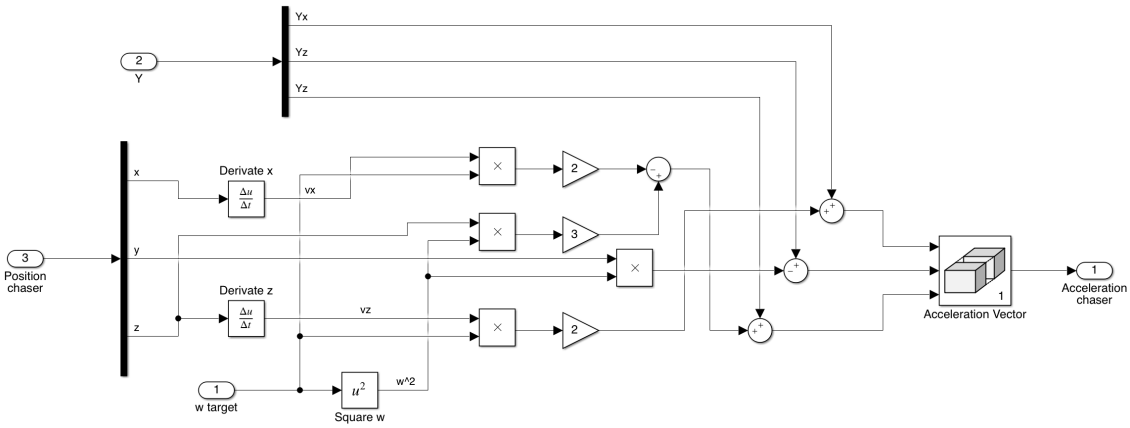

Figure A.2: Hill's equations model

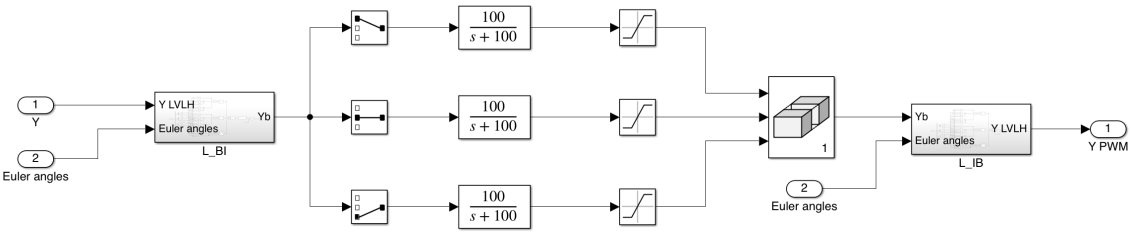

Figure A.3: Hill's equations model

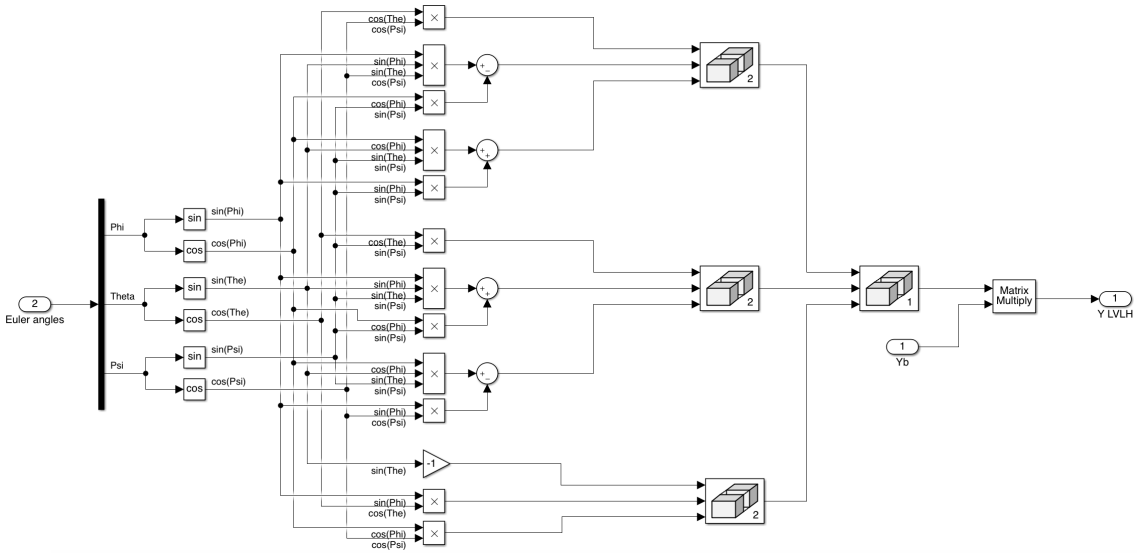

Figure A.4: Body frame to LVLH frame model

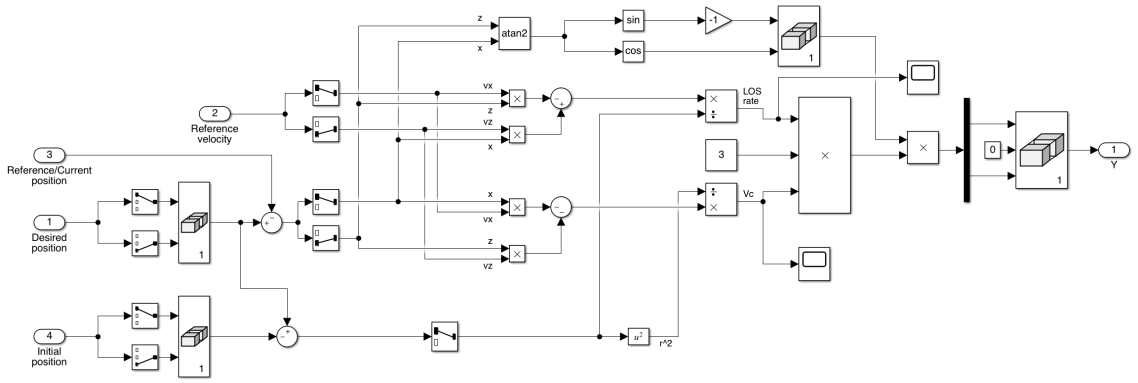

Figure A.5: PNG acceleration command model

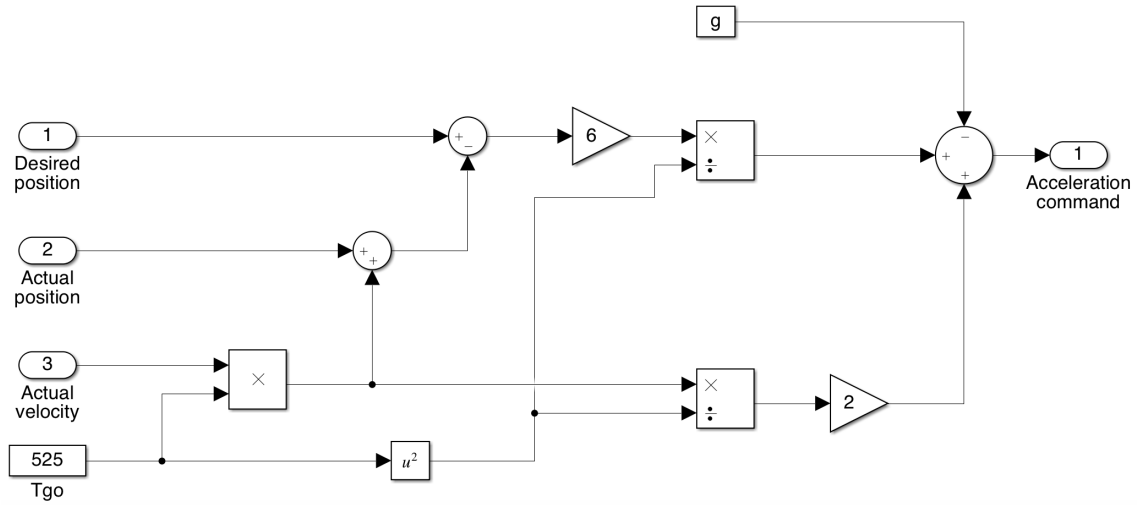

Figure A.6: CTVG acceleration command model

A.2. Attitude control models

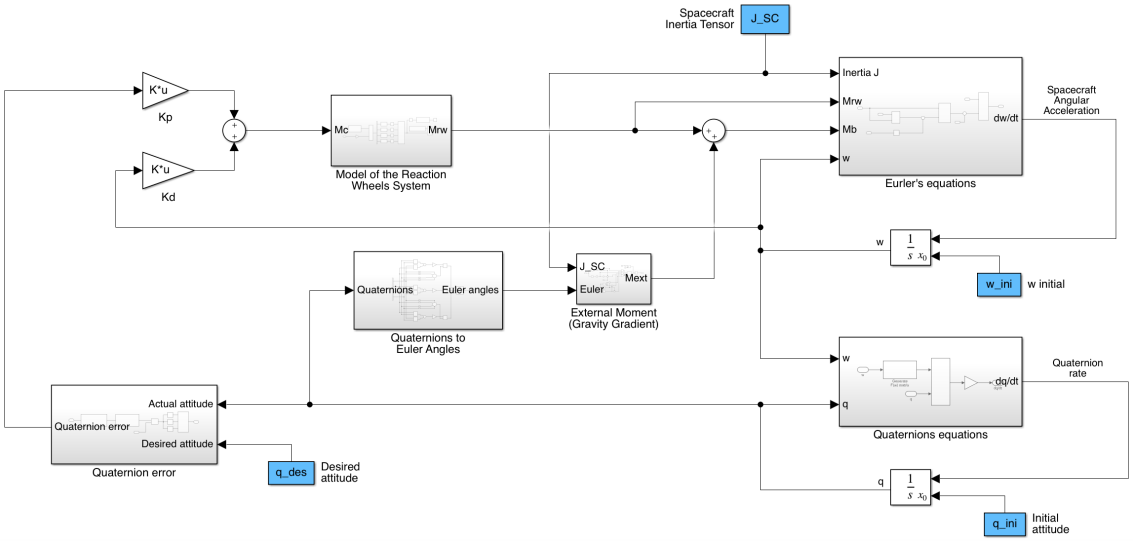

Figure A.7: Attitude control model

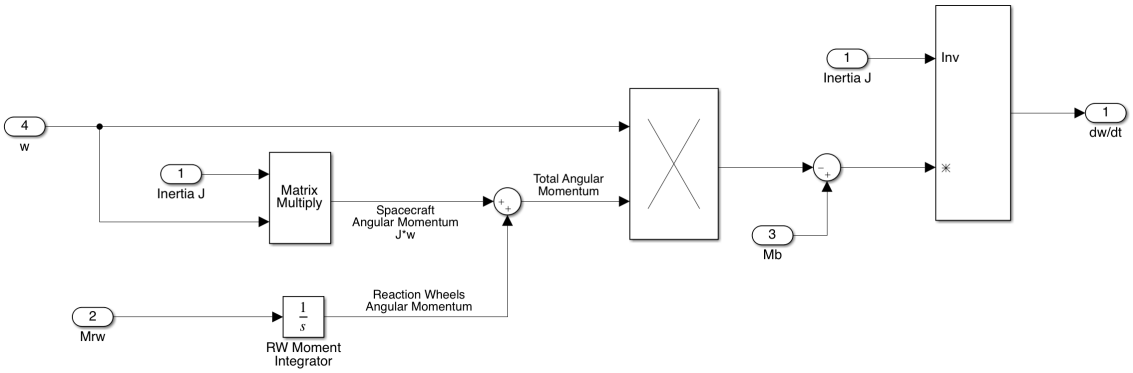

Figure A.8: Euler's equations model

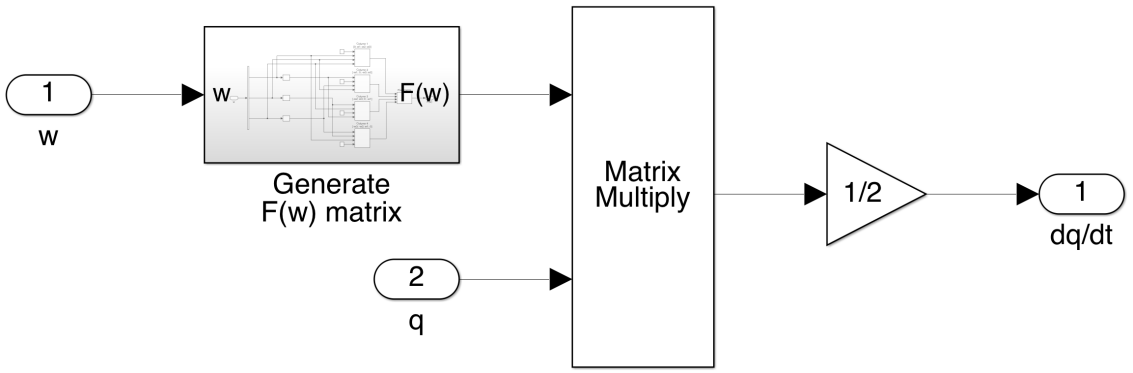

Figure A.9: Kinematic equations with quaternions model

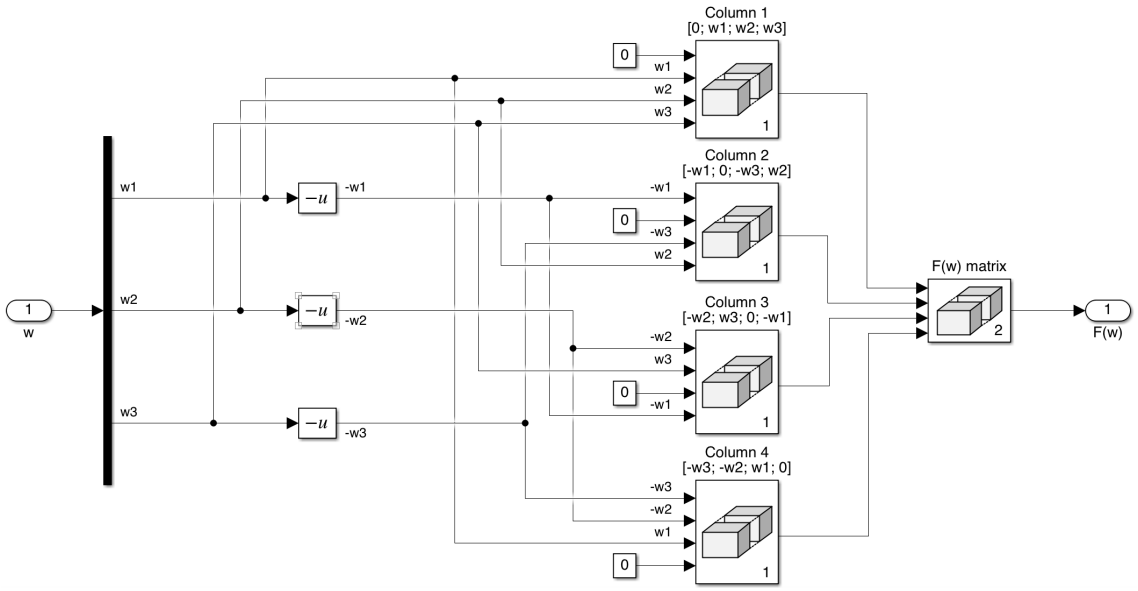

Figure A.10: $F_q(\omega)$ matrix model

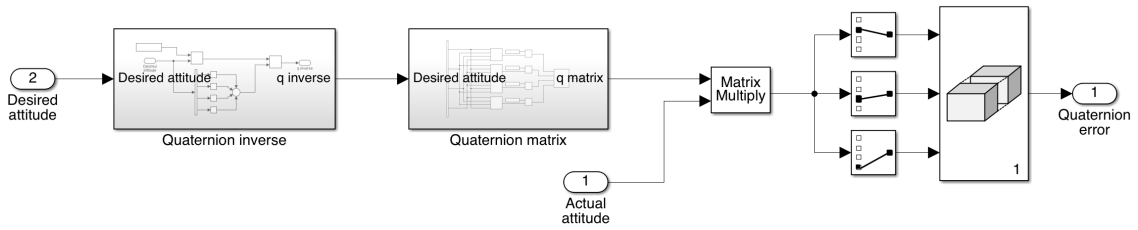

Figure A.11: Quaternions error model

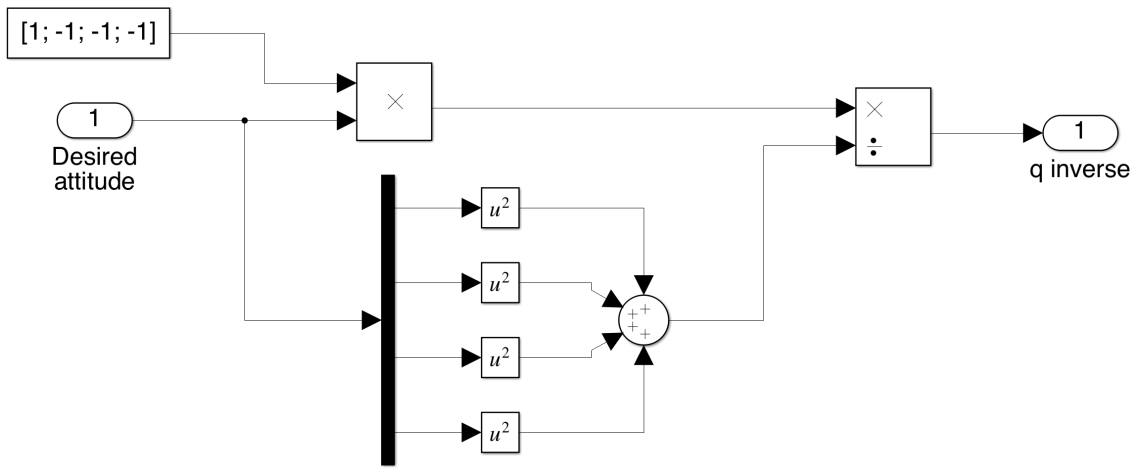

Figure A.12: Quaternion inverse model

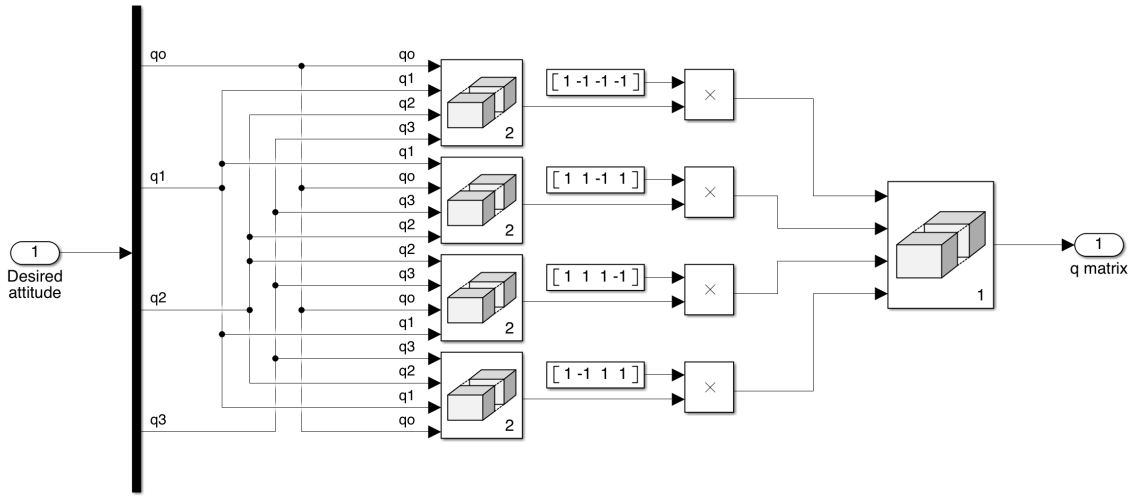

Figure A.13: Quaternion matrix model

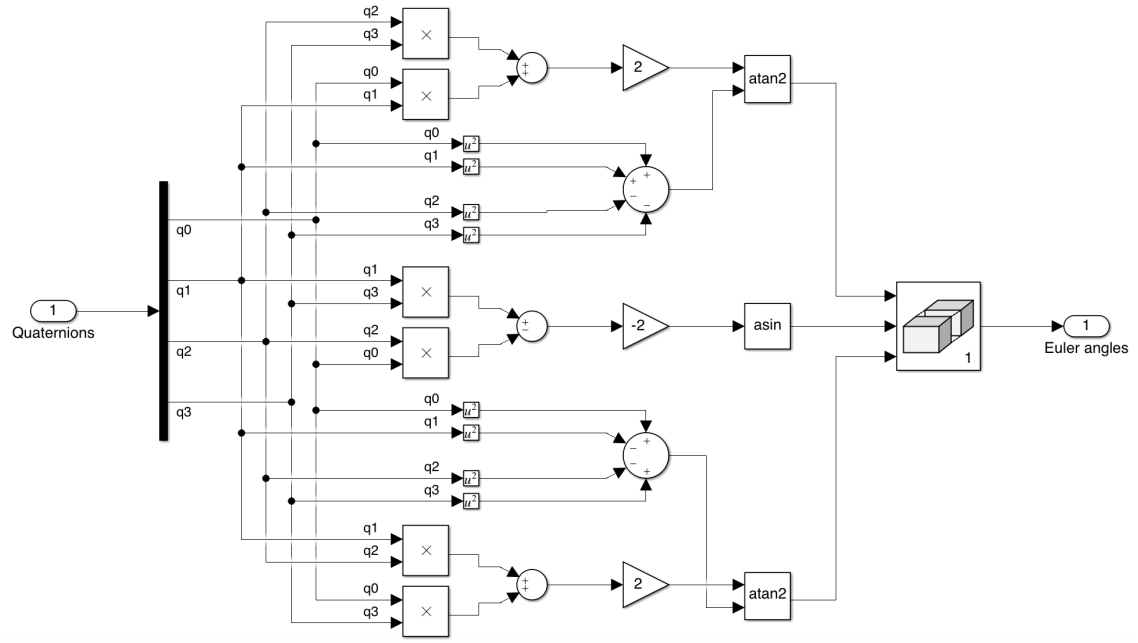

Figure A.14: Quaternion to Euler angles model

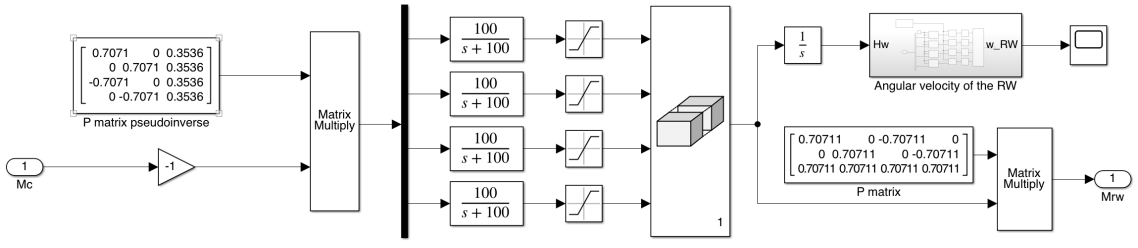

Figure A.15: Reaction wheels model